

1 **The FW2.2/CNR protein regulates cell-to-cell communication in tomato by**  
2 **modulating callose deposition at plasmodesmata**

3

4 **Short Title: FW2.2/CNR regulates cell-to-cell communication**

5

6 Arthur Beauchet<sup>a†¶</sup>, Norbert Bollier<sup>a†</sup>, Magali Grison<sup>b</sup>, Valérie Rofidal<sup>c</sup>, Frédéric  
7 Gévaudant<sup>a</sup>, Emmanuelle Bayer<sup>b</sup>, Nathalie Gonzalez<sup>a,1</sup> and Christian Chevalier<sup>a,1</sup>

8 <sup>a</sup> Université Bordeaux, INRAE, UMR1332 Biologie du Fruit et Pathologie, F-33140  
9 Villenave d'Ornon, France

10 <sup>b</sup> Université Bordeaux, CNRS, UMR5200 Laboratoire de Biogénèse Membranaire, F-  
11 33140 Villenave d'Ornon, France

12 <sup>c</sup> IPSiM, Université Montpellier, CNRS, INRAE, Institut Sup Agro, F-34060  
13 Montpellier, France

14 <sup>1</sup> Correspondence: [nathalie.gonzalez@inrae.fr](mailto:nathalie.gonzalez@inrae.fr) and [christian.chevalier@inrae.fr](mailto:christian.chevalier@inrae.fr)

15 <sup>†</sup> A.B. and N.B. contributed equally to this work

16 <sup>¶</sup> Present address: VIB-UGent for Plant Systems Biology, Ghent University, 9052  
17 Ghent, Belgium

18

19 ORCID IDs: 0000-0003-3704-3795 (A.B.); 0000-0003-0537-4151 (N.B.); 0000-0002-  
20 3080-3686 (M.G.); 0000-0001-9777-2856 (F.G.); 0000-0001-8642-5293 (E.B.); 0000-  
21 0002-3946-1758 (N.G.); 0000-0002-5727-6206 (C.C.)

22

23 The authors responsible for distribution of materials integral to the findings presented  
24 in this article in accordance with the policy described in the Instructions for Authors  
25 (<https://academic.oup.com/plcell/pages/General-Instructions>) are: Nathalie Gonzalez  
26 (nathalie.gonzalez@inrae.fr) and Christian Chevalier (christian.chevalier@inrae.fr).

27

28

29 **Abstract**

30 The *FW2.2* gene is the founding member of the *CELL NUMBER REGULATOR*  
31 (*CNR*) gene family. More than 20 years ago, *FW2.2* was the first cloned gene  
32 underlying a Quantitative Trait Locus (QTL) governing fruit size/weight in tomato.  
33 However, despite this discovery, the molecular mechanisms by which *FW2.2* acts as  
34 a negative regulator of cell divisions during fruit growth remain undeciphered. In the  
35 present study, we confirm that *FW2.2* is a transmembrane spanning protein, whose  
36 both N- and C-terminal ends are facing the apoplast. We unexpectedly found that  
37 *FW2.2* is located at plasmodesmata (PD). *FW2.2* participates in the spatiotemporal  
38 regulation of callose deposition at PD via an interaction with Callose Synthases,  
39 which suggests a regulatory role in cell-to-cell communication by modulating PD  
40 transport capacity and trafficking of signaling molecules during fruit development.

41

42 **INTRODUCTION**

43 The tight coordination of developmental processes such as cell division, cell  
44 expansion and cell differentiation, is pivotal for proper plant growth at the whole  
45 organismal, organ and tissue level. Unravelling the genes that contribute to impact  
46 plant yield and biomass, and improve agronomical quality traits, is thus a major goal  
47 of plant biology and agronomy. In the particular case of tomato fruit size  
48 determination, nearly 30 Quantitative Trait Loci (QTL) governing fruit size/weight  
49 have been identified (Grandillo et al., 1999; Lippman and Tanksley, 2001; van der  
50 Knaap and Tanksley, 2003). However, the molecular basis governing these QTLs  
51 remains mostly undeciphered, and only three major genes underlying such QTLs in  
52 tomato have been identified and cloned so far (Frary et al., 2000; Chakrabarti et al.,  
53 2013; Mu et al., 2017).

54 *FW2.2* was the first cloned gene underlying a QTL related to fruit size in tomato  
55 (Alpert et al., 1995; Frary et al., 2000). The encoded protein *FW2.2* was defined as a  
56 major negative regulator of cell divisions in young developing fruit, and thus  
57 impacting fruit size (Frary et al., 2000; Cong et al., 2002; Liu et al., 2003; Nesbitt and  
58 Tanksley, 2001; Baldet et al., 2006). *FW2.2* was the founding member of the *CELL*  
59 *NUMBER REGULATOR*/*FW2.2*-Like (*CNR*/*FWL*) protein family (Guo et al., 2010),  
60 whose function in organ size control seems to be conserved in both monocotyledon  
61 and dicotyledon plants (for a review, see Beauchet et al., 2021). Members of this

62 protein family possess a conserved PLAC8 (Placenta-specific gene 8 protein) domain  
63 (Galaviz-Hernandez et al., 2003), which is composed of one or two hydrophobic  
64 segments, predicted to form transmembrane (TM) helices (Song et al., 2004). The  
65 hydrophobic segments are characterized by the presence of conserved Cys-rich  
66 motifs of the type CLXXXXCPC or CCXXXXCPC, separated by a variable region and  
67 located at the N-terminal part of a first TM domain (Beauchet et al., 2021). A  
68 localization at the plasma membrane (PM) was indeed demonstrated for the tomato  
69 FW2.2 protein (Cong and Tanksley, 2006), as well as for CNR/FWL homologous  
70 proteins in various fruit species such as eggplant, pepper, Physalis, avocado, cherry  
71 (Dahan et al., 2010; De Franceschi et al., 2013; Doganlar et al., 2002; Li and He,  
72 2015), but also in *Arabidopsis*, cereal and leguminous species (Libault et al., 2010;  
73 Guo et al., 2010; Song et al., 2010; Xu et al., 2013). In soybean, the CNR/FWL  
74 protein GmFWL1 was shown to display a punctate localization in plasma membrane  
75 nanodomains, which supported its ability to interact with membrane nanodomain-  
76 associated proteins such as flotillins, prohibitins, remorins, proton- and vacuolar-  
77 ATPases, receptor kinases, leucine-rich repeat proteins (Qiao et al., 2017).

78 Despite the seemingly conserved roles in cell division and organ size control  
79 (Beauchet et al., 2021), the precise physiological and biochemical function of FW2.2  
80 or its CNR/FWL homologues remains unknown so far. The conceptual question in  
81 studying the functional role of FW2.2 and CNR/FWL is thus how to conciliate a  
82 localization at the plasma membrane and nanodomains with a spatial and temporal  
83 control of cell divisions in order to regulate plant organ growth.

84 In plants, important biological functions are associated to membrane  
85 nanodomains. Plasmodesmata (PD) belong to such PM nanodomains. PD are cell  
86 wall- and membrane-spanning channels, which provide direct cytosolic continuity to  
87 mediate symplastic communication between cells (Maule et al., 2011; Petit et al.,  
88 2020). PD control cell-to-cell movements of different mobile signalling molecules  
89 (Van Norman et al., 2011; Gallagher et al., 2014), and thus regulate the connection  
90 between cells ensuring both local and systemic responses to biotic and abiotic  
91 stresses, the exchange of nutrients and organs, regulating symbiotic interactions and  
92 supporting the coordination of developmental processes (Gaudioso-Pedraza et al.,  
93 2018; Grison et al., 2019; Han et al., 2014a; O'Lexy et al., 2018; Yan et al., 2019).  
94 Hormones, metabolites, non-cell autonomous proteins, including transcription factors  
95 (TFs), and small RNAs represent such mobile signalling molecules, trafficking from

96 cell-to-cell via PD. The symplastic communication via PD is finely tuned by  
97 developmental or environmental factors, which exert a control on the size exclusion  
98 limit of PD. Among these factors, the deposition of callose, a (1,3)- $\beta$ -glucan polymer,  
99 regulated by the antagonistic action of callose synthases and  $\beta$ -glucanases, is a  
100 major process that constricts the PD channel, and thus decreases the aperture of PD  
101 (Amsbury et al., 2018). Consequently, the balance between callose deposition and  
102 degradation at the neck region of PD plays a major role in the regulation of cell-to-cell  
103 communication.

104 In an effort to unravel the cellular and molecular mechanisms sustaining the mode  
105 of action of FW2.2 in tomato, we re-investigated its subcellular localization *in planta*.  
106 We unexpectedly found that FW2.2 protein not only associates with bulk PM but also  
107 clusters at PD in the different tissues we examined. We further show that FW2.2  
108 modulates the functionality of PD by modifying callose levels. FW2.2-induced  
109 regulation of callose most likely occurs through direct interaction with PD-associated  
110 Callose Synthases. Our data shed light on an unforeseen function of FW2.2 in  
111 modulating cell-to-cell communication in tomato.

112

## 113 **RESULTS**

### 114 **FW2.2 localizes at the plasma membrane with the N- and C-terminal parts 115 facing the apoplast.**

116 The first and only demonstration that FW2.2 addresses the PM was provided by  
117 transient expression analysis using onion epidermal cells and tomato young leaf cells  
118 (Cong and Tanksley, 2006). This PM localization is conferred by the two  
119 transmembrane domains (TMD) contained in the PLAC8 domain, but the exact  
120 topology of the FW2.2 protein at PM is still uncharacterized.

121 First, we confirmed the PM localization of FW2.2, using transient expression in  
122 *Nicotiana benthamiana* leaves (Xie et al., 2017). FW2.2 fused to GFP either at its C-  
123 terminus or N-terminus was indeed addressed to the PM (**Figure 1A**). To investigate  
124 the mode of action of FW2.2 at PM, we then study the topology of FW2.2 by using a  
125 Bi-molecular Fluorescent Complementation (BiFC) approach that had been validated  
126 for PM-located proteins (Thomas et al., 2008). The FW2.2 protein was fused at its N-  
127 or C-terminus to the truncated version of GFP, namely GFP11, which contains the  
128 last and eleventh  $\beta$ -sheet. The GFP11-FW2.2 or FW2.2-GFP11 construct was then

129 co-expressed with the cytosolic truncated version of the GFP, namely GFP1-10  
130 containing the first ten  $\beta$ -sheets. Alternatively, the GFP11-FW2.2 or FW2.2-GFP11  
131 construct was co-expressed with a secreted apoplastic version of GFP1-10, namely  
132 SP-GFP1-10 (SP for Signal Peptide of the Arabidopsis PR1 protein; At2g14610). As  
133 a positive control for a cytosolic interaction, we fused the GFP11 to the C-terminal  
134 part of the PM located protein Lti6b (Low-temperature induced 6b protein;  
135 At3g05890) that faces the cytosol (Martiniere et al., 2012), and co-infiltrated this  
136 construct with the GFP1-10. The Lti6b-GFP11 construct was thus expected to be  
137 unable to interact with the apoplastic SP-GFP1-10.

138 A strong GFP signal was observed when the Lti6b-GFP11 was co-expressed with  
139 the cytosolic GFP1-10, and no signal was observed when co-expressed with the  
140 apoplastic SP-GFP1-10, which validated the BiFC approach (**Figure 1B**). The co-  
141 expression of FW2.2 fused to GFP11 at both its C- and N-terminus with the cytosolic  
142 GFP1-10, did not result in any visible fluorescence signal. On the contrary, the co-  
143 expression of FW2.2 fused to GFP11 with the apoplastic SP-GFP1-10 resulted in a  
144 strong GFP signal at the PM (**Figure 1B**). Therefore, we confirmed that FW2.2 is  
145 associated to PM as previously reported (Cong and Tanksley, 2006), but we provided  
146 evidence that the two TMDs within FW2.2 drives a protein topology where the N- and  
147 C-terminus are facing the apoplast.

148 To confirm this topology, we performed a second transient expression assays,  
149 using a system of apoplastic and cytoplasmic pH sensors described by Martinière et  
150 al. (2018). This system takes advantage of the pH-sensitive ratiometric behavior of  
151 the protein pHluorin (pHGFP), whose emitted fluorescence differs according to its  
152 location in the cytosol or the apoplast, depending on their respective pH value of ~7.5  
153 or ~6.0. Following agro-infiltration of *N. benthamiana* leaves, the fluorescence  
154 emitted by pHGFP is recorded after an excitation wavelength of 405 nm and 488 nm,  
155 to establish a 405/488 fluorescence intensity ratio, indicative of pH differences. The  
156 discrimination between the apoplastic and cytosolic 405/488 ratio was made possible  
157 by the use of the following constructs. The apoplastic membrane pH sensor pHGFP-  
158 PM-Apo resulted from the fusion of pHGFP with the TMD of the PM-localized protein  
159 TM23 (Brandizzi et al., 2002), and the cytosolic membrane pH sensor pHGFP-PM-  
160 Cyto corresponded to the fusion of pHGFP with the C-terminal farnesylation  
161 sequence of Ras which is anchored to the PM (Martinière et al., 2018).

162 As expected, the 405/488 nm fluorescence ratio measured in *N. benthamiana* cells  
163 was higher for the pHGFP-PM-Cyto (median=2.2) when compared to that for  
164 pHGFP-PM-Apo (median=1.3), revealing the higher pH of the cytosolic compartment  
165 than that of apoplast (**Figure 1C**). The 405/488 nm fluorescence ratio was then  
166 measured in cells transformed with FW2.2 fused with the pHGFP either at its N-  
167 terminal or C-terminal end. It was shown to be very close to the fluorescence ratio  
168 measured with the pHGFP-PM-Apo (median=1.3), thus demonstrating unequivocally  
169 that the N- and C-terminal parts of FW2.2 are facing the apoplast (**Figure 1B**).  
170

### 171 **FW2.2 is enriched at plasmodesmata**

172 To go deeper into the study of the FW2.2 subcellular localization, we generated  
173 stable transgenic lines expressing FW2.2 fused to YFP at its C-terminal end under  
174 the control of the Cauliflower Mosaic Virus (CaMV) 35S promoter (referred to as  
175 35S::FW2.2-YFP plants), in the cultivated tomato variety Ailsa Craig (AC). In these  
176 plants, the emitted fluorescence associated to YFP was highly detectable in roots  
177 and leaves, and in reproductive organs, namely flowers and fruits (**Supplemental**  
178 **Figure 1A**). The localization of FW2.2-YFP at the PM was confirmed in all tissues  
179 investigated, namely in roots and fruit pericarp (**Figure 2A**), according to a pattern of  
180 punctate spots at the cell periphery, suggesting that FW2.2-YFP was enriched at  
181 nanodomains as observed previously for the soybean ortholog GmFWL1 (Qiao et al.,  
182 2017). The same tissue preparations were then stained with aniline blue (AB) to  
183 reveal callose deposition, as a marker of PD. The fluorescent dots revealing FW2.2-  
184 YFP co-localised with AB staining, at pit field junctions, as shown by the overlapping  
185 signal intensity plots (**Figure 2A**), thus indicating a localization at PD. It is noteworthy  
186 that the localization of FW2.2 at PD was independent from the position of YFP at the  
187 C-terminal or N-terminal end of the protein, since we obtained similar results using a  
188 35S::YFP-FW2.2 construct (**Supplemental Figure 1B**). The enrichment of FW2.2 at  
189 PD was quantified by measuring the plasmodesmata enrichment ratio, named 'PD  
190 index', corresponding to the FW2.2-YFP fluorescence intensity at PD vs that at the  
191 cell periphery, as previously described (Brault et al., 2019; Grison et al., 2019). As a  
192 control, root and fruit pericarp tissues from WT plants were stained with FM4.64, a  
193 PM-specific dye (Bolte et al., 2004), together with AB to measure the PD index. While  
194 the PD index in controls was equal to 1 regardless of the tissue tested, a high PD-

195 index ranging from 1.7 to 1.9 was measured in root and pericarp cells of 35S::FW2.2-  
196 YFP plants, (**Figure 2B**), thus demonstrating that FW2.2 was enriched at PD.

197

198 **The overexpression of FW2.2 in leaves enhances cell-to-cell diffusion capacity**

199 Since FW2.2 localizes at PD, we hypothesized that it could contribute to a function  
200 associated to cell-to-cell communication. To test this hypothesis, a new set of gain-of-  
201 function plants were generated in the tomato cultivar AC, as to overexpress *FW2.2*  
202 constitutively and ectopically, under the control the 35S promoter (referred to as  
203 35S::FW2.2). Three lines were selected with medium- (2-fold more) to very high  
204 levels (50-fold more) of *FW2.2* overexpression in 5 DPA fruits, a stage when the  
205 endogenous *FW2.2* expression is at its maximum (**Supplemental Figure 2**). In  
206 parallel, loss-of-function plants were generated using the CRISPR/Cas9 technology.  
207 To knock out *FW2.2*, two single-guide RNAs (sgRNAs) were designed as close as  
208 possible to the start codon of the coding sequence to create a frameshift or an early  
209 stop codon resulting in a dysfunctional FW2.2 protein in which the PLAC8 domain is  
210 missing (**Supplemental Figure 3**). Three different homozygous lines were selected,  
211 and referred to as *CR-fw2.2* hereafter.

212 In all three independent 35S::FW2.2 overexpressing lines, a significant reduction  
213 in mean leaf surface was observed, from 33% to 42% compared to that in WT  
214 (**Figure 3A**). This reduction in leaf surface was not due to any alteration of cell size,  
215 as the leaf epidermal cell density, used as a proxy for cell size, was unaffected  
216 (**Figure 3B**). No growth-related phenotype was observed in leaves of *CR-fw2.2*  
217 plants, which was expected as *FW2.2* is not naturally expressed in leaves  
218 (**Supplemental Figure 2B**).

219 We next investigated whether the overexpression of *FW2.2* in leaves could affect  
220 the permeability of PD, and consequently the cell-to-cell communication. The PD  
221 permeability in WT, 35S::FW2.2 and *CR-fw2.2* lines was compared by performing  
222 “Drop-ANd-See” (DANS) quantitative assays (Cui et al., 2015), using the membrane-  
223 permeable, non-fluorescent dye Carboxy-Fluorescein DiAcetate (CFDA). DANS  
224 assays are based on the ability of cell to uptake CFDA rapidly; intracellular esterases  
225 then cleave CFDA into fluorescent but membrane-impermeable Carboxy-Fluorescein  
226 (CF), and CF diffuses symplastically into the neighbouring cells only via PD. To our  
227 knowledge, the use of this technique has never been reported in tomato. We first

228 checked that DANS assays are functional in tomato using leaflets of 4 weeks-old  
229 plants (**Supplemental Figure 4A**).

230 In *Arabidopsis*, a pre-treatment with 10 mM H<sub>2</sub>O<sub>2</sub> alters PD permeability through an  
231 increase in callose deposition (Cui and Lee, 2016). Such an effect was also observed  
232 in tomato WT leaves, as revealed by the reduction in CF signal intensity compared to  
233 mock-treated leaves, thus indicating a decrease in PD permeability affecting the cell-  
234 to-cell movement of CF in tomato leaves (**Figure 3C-D**). We then examined whether  
235 gain- or loss-of-function of *FW2.2* alters cell-to-cell communication. The CF signal  
236 intensity was increased (from 20 to 30%) in all overexpressing 35S::*FW2.2* lines  
237 compared to that in WT, suggesting an increased PD permeability (**Figure 3C-D**).  
238 Interestingly, the H<sub>2</sub>O<sub>2</sub> treatment which increases callose deposition in WT and  
239 thereby decreases PD permeability, had no effect on the 35S::*FW2.2* lines,  
240 compared to the mock treatment. Hence, not only the overexpression of *FW2.2* in  
241 leaves increased PD permeability, but it also inhibited the negative effects of H<sub>2</sub>O<sub>2</sub> on  
242 it. On the contrary, the CF signal intensity in *CR-fw2.2* lines was similar to that in WT  
243 (**Figure 3C-D**), showing no difference in CF diffusion, which suggests that the PD  
244 permeability was not affected. This absence of effects on PD permeability in *CR-*  
245 *fw2.2* lines can be explained by the absence of endogenous *FW2.2* expression in  
246 leaves, as mentioned above. It also correlates with the absence of any alteration in  
247 epidermal cell size in 35S::*FW2.2* and *CR-fw2.2* lines (**Supplemental Figure 4B**).  
248 Therefore, the observed difference in CF diffusion was the result of the  
249 overexpression of *FW2.2* in tomato leaves, which induced a modification in the cell-  
250 to-cell communication status, as revealed by the altered PD permeability.  
251

## 252 **FW2.2 affects the callose deposition at PD in leaves**

253 A key mechanism for the regulation of PD aperture, and therefore for intercellular flux  
254 of signalling molecules, involves the accumulation of the cell wall polysaccharide  
255 callose at the neck regions of PD (Amsbury et al., 2018). To verify whether the  
256 increase in cell-to-cell diffusion mediated by the overexpression of *FW2.2* was due to  
257 a modified level of callose accumulation, the levels of callose at PD were measured  
258 in leaves from WT, 35S::*FW2.2* and *CR-fw2.2* plants, following a pre-treatment with  
259 or without H<sub>2</sub>O<sub>2</sub>. The levels of callose were quantified by immunofluorescence  
260 labelling using a callose-specific antibody as illustrated for WT in **Figure 4A**, and the  
261 signal intensity was subsequently quantified as a proxy of callose deposition at PD

262 (Figure 4B), as commonly used (Grison et al., 2019; Platret et al., 2022; Wang et al.,  
263 2023). Compared to control conditions (mock treatment), the signal intensity for  
264 callose in WT leaves treated with H<sub>2</sub>O<sub>2</sub> was increased, correlating with DANS assays  
265 showing decreased cell-cell communication. The immunofluorescence intensity in the  
266 35S::FW2.2 leaves was decreased when compared to that in WT, indicating that less  
267 callose was deposited, in the absence of any alteration in cell size and leaf thickness  
268 as verified before (Figure 3B and Supplemental Figure 4). In response to H<sub>2</sub>O<sub>2</sub>, the  
269 levels of callose deposition in 35S::FW2.2 leaves also increased, but to a much lower  
270 extent than in WT (Figure 4B). On the contrary, the levels of callose deposition in  
271 CR-fw2.2 leaves with or without H<sub>2</sub>O<sub>2</sub> were highly similar to that in WT, in accordance  
272 with the absence of phenotype when FW2.2 is mutated (Figure 3).

273 These results clearly indicated that FW2.2 alters the process of callose deposition  
274 at PD.

275

#### 276 FW2.2 regulates negatively callose deposition at PD in fruit pericarp

277 Since FW2.2 was found as a major regulator of fruit weight, we next examined  
278 whether the misexpression of FW2.2 would affect the level of callose deposition at  
279 PD in fruit pericarp tissue.

280 At a macroscopic level, among the three selected overexpressing lines, a  
281 significant reduction in mean fruit weight was observed for the 35S::FW2.2-1 and  
282 35S::FW2.2-3 lines (according to an average increase of 19.6% and 11.3%  
283 respectively) (Figure 5A). The mean fruit weight in the three CR-fw2.2 loss-of  
284 function plants was higher than that of the WT (7.2%, 7.1% et 6.3% respectively).  
285 However, these differences were not statistically significant, because of a high  
286 variability in fruit weight values. In addition, there was no modification in pericarp  
287 thickness in mature fruits from the three 35S::FW2.2 lines compared to WT fruits,  
288 while pericarp from CR-fw2.2 fruits appeared thinner (Figure 5B). Related to fruit  
289 structure, fruits from gain- and loss-of-function plants were all affected for the number  
290 of locules to various degrees (Figure 5C). More fruits with less than 3 locules were  
291 encountered in the overexpressing 35S::FW2.2 lines, while fruits with 4 and even  
292 more locules were observed in CR-fw2.2 lines, compared to WT fruits from the AC  
293 cultivar which usually contain 3 locules. This converse impact on the number of fruit  
294 locules in the gain- and loss-of-function plants suggests that cell divisions have been

295 impacted in the floral meristem (FM) termination process, through the increased or  
296 repressed negative regulatory effect in 35S::FW2.2 or CR-fw2.2 lines respectively.

297 The level of callose deposition was then investigated on pericarp sections of fruits  
298 from the 35S::FW2.2 and CR-fw2.2 plants harvested at 5 and 15 DPA (**Figure 5D**).  
299 These two different developmental stages were chosen because FW2.2 is highly  
300 expressed in the pericarp of 5 DPA fruit and much less at 15 DPA (**Supplemental**  
301 **Figure 2B**). At both 5 and 15 DPA, the immunofluorescence signal intensity in the  
302 pericarp of 35S::FW2.2 fruits was decreased when compared to that in WT,  
303 indicating that the level of callose deposition was reduced (**Figure 5D-E**). On the  
304 contrary, the immunofluorescence signal intensity in the pericarp of CR-fw2.2 fruits at  
305 both 5 and 15 DPA was increased significantly when compared to that in WT, thus  
306 revealing a higher level of callose deposition. Interestingly, the increase in callose  
307 deposition observed at 15 DPA in pericarp sections from CR-fw2.2 fruits was less  
308 pronounced than at 5 DPA, and almost identical to that in WT. This can be explained  
309 by the very low expression of FW2.2 in 15 DPA fruits (**Supplemental Figure 2B**),  
310 and thus the absence of any loss-of-function effect from the CRISPR-Cas9 construct  
311 on FW2.2 at this developmental stage.

312 Cell perimeters were measured for all genotypes in all the different cell layers  
313 composing the fruit pericarp at 5 DPA, and in the mesocarp at 15 DPA, to ascertain  
314 that these differences in callose deposition was not due to any heterogeneity in cell  
315 size, and thus in the density of cell walls. The cell perimeter was comparable in all  
316 WT, 35S::FW2.2 and CR-fw2.2 lines, with only slightly smaller values in some cases,  
317 especially in the internal part of the mesocarp (**Supplemental Figure 5**). Hence, the  
318 observed differences in callose deposition did originate from the effects of FW2.2  
319 gain- and loss-of-function, demonstrating that FW2.2 regulates negatively the  
320 process of callose deposition at PD within fruit pericarp.

321

### 322 **FW2.2 interacts physically with Callose Synthases**

323 To go deeper into the functional and biochemical characterization of FW2.2, an *in*  
324 *vivo* approach using immunoprecipitation followed by tandem-mass spectrometry (IP-  
325 MS/MS) was performed to identify interacting protein partners of FW2.2 inside the  
326 pericarp from 35S::FW2.2-YFP fruits harvested at 10 DPA. Since FW2.2 is still  
327 expressed endogenously at this developmental stage, it was therefore expected that  
328 its natural interacting proteins would be present in the protein extracts. The IP-

329 MS/MS experiment resulted in the identification of 662 proteins interacting with  
330 FW2.2, which were enriched in the 35S::FW2.2-YFP sample when compared to WT  
331 (**Figure 6A, Supplemental Data Set 1**). To identify potential PD-localized candidates  
332 in relation with FW2.2 function, we compared this list with a tentative PD proteome  
333 from tomato made of a total of 400 proteins corresponding to the deduced orthologs  
334 of the 115 proteins constituting the refined PD proteome from Arabidopsis published  
335 by Brault *et al.* (2019). Seventeen proteins were found overlapping between the two  
336 proteomes (**Figure 6B**). Three distinct classes of proteins, all key regulators of cell-  
337 to-cell signalling in plants, represented almost two thirds of the identified proteins  
338 (**Figure 6C**): i) two proteins of the C2 calcium/lipid-binding phosphoribosyl  
339 transferase family (Solyc01g080430 and Solyc01g094410), belonging to the large  
340 family of multiple C2 domains and transmembrane region proteins (MCTP) (Brault *et*  
341 *al.*, 2019); ii) three proteins of Leucine-Rich Repeat Receptor-Like kinases (LRR-  
342 RLKs) family (Solyc03g111670, Solyc06g082610 and Solyc05g052350) (Wei *et al.*,  
343 2015); iii) six different Callose Synthases (CaLS), which were identified based on their  
344 phylogenetic proximity to Arabidopsis counterparts, namely SICaLS1  
345 (Solyc01g006350), SICaLS3a (Solyc01g006370), SICaLS3b (Solyc01g073750),  
346 SICaLS9 (Solyc01g006360), SICaLS10a (Solyc03g111570) and SICaLS12  
347 (Solyc07g053980) (**Supplemental Figure 6A**). The preferential interaction of FW2.2  
348 with Callose synthases in 10 DPA fruits was thus fully relevant with its  
349 aforementioned role in regulating callose deposition at PD in the pericarp. RT-qPCR  
350 analyses confirmed that these 6 CaLS genes were expressed in WT fruit pericarp at  
351 10 DPA (**Supplemental Figure 6B**). In addition, there was no significant change in  
352 the expression level of the 6 CaLS genes in tomato leaves and fruits at 5 and 15 DPA  
353 from the FW2.2 loss- and gain-of-function plants except for SICaLS12  
354 (Solyc07g053980) whose expression was lower in leaves and 5 DPA fruits of  
355 35S::FW2.2 and higher in 5 DPA fruits of CR-fw2.2 (**Supplemental Figure 7**).  
356 Therefore, the preferential interaction between FW2.2 and the six CaLS proteins is not  
357 related to an increase in CaLS gene expression in the 35S::FW2.2-YFP plants, and  
358 ultimately to an increased translation, but to the endogenous level of CaLS in the  
359 protein extracts of 10 DPA fruits used for the IP experiment.

360 These results thus support the functional role of FW2.2 on PD permeability and  
361 cell-to-cell communication, via an interaction with Callose synthases, which may  
362 potentially modulate their catalytic activity.

363

364 **DISCUSSION**

365 FW2.2 was the first gene underlying a QTL related to fruit size to be cloned in tomato  
366 (Frary et al., 2000). It is by far the major QTL of such type, as it accounts for as much  
367 as a 30% difference in fruit fresh weight between domesticated (large-fruited)  
368 tomatoes and their wild (small-fruited) relatives (Frary et al., 2000; Grandillo et al.,  
369 1999). Most wild -small fruited- tomatoes (if not all) possess 'small-fruit' alleles;  
370 conversely all domesticated/cultivated -large fruited- tomatoes possess 'large-fruit'  
371 alleles (Bianca et al., 2015). Comparative sequence analysis of FW2.2 from the  
372 large- and small-fruited alleles indicated that the *FW2.2* effects on fruit size do not  
373 originate from differences in the sequence and structure of the protein, but rather  
374 from the timing of its transcription (heterochronic changes) and the overall quantity of  
375 transcripts in the fruit (Cong et al., 2002). The 'large-fruit' allele is rapidly transcribed  
376 to reach a peak of expression around 5 DPA, whereas the 'small-fruit' allele is  
377 transcribed more slowly and displays its maximum of expression nearly a week later  
378 (12 to 15 DPA), reaching almost twice the mRNA level observed in large-fruit allele  
379 (Cong et al., 2002). Since this difference in timing of expression was found inversely  
380 correlated to the mitotic activity, FW2.2 was defined as a negative regulator of cell  
381 divisions in pre-anthesis ovary and developing fruit, thus modulating final fruit size  
382 (Frary et al., 2000; Cong et al., 2002). Such a function in regulating organ size by  
383 modulating cell number was found conserved for many other plant orthologues of  
384 FW2.2 (Beauchet et al., 2021), which led to the attribution of the CELL NUMBER  
385 REGULATOR (CNR) protein family name (Guo et al., 2010). Members of the CNR  
386 protein family are targeted to the PM, due to the presence of the PLAC8 domain  
387 (Beauchet et al., 2021). However, the precise biological function and mechanism of  
388 action of membrane-embedded FW2.2 and CNRs in controlling organ size via the  
389 regulation of cell divisions remained totally elusive so far.

390

391 **FW2.2 regulates cell-to-cell diffusion by modulating callose deposition at  
392 plasmodesmata**

393 It was long known that FW2.2 is a plasma membrane-located protein (Cong and  
394 Tanksley, 2006). Using transient expression in tobacco leaves and stable  
395 transformants in the tomato AC cultivar, we confirmed this PM localization for FW2.2

396 (**Figures 1-2**). The topology of FW2.2 within the PM was established and revealed  
397 that the N- and C-terminal regions are extracellular, thus facing the apoplast, while  
398 the protein loop in-between the two TMDs is cytoplasmic (**Figure 1**). These results  
399 were in full agreement with a topological model predicted for PfCNR1, the FW2.2  
400 putative orthologue from *Physalis floridana*, which displays a high degree of  
401 homology with FW2.2 (Li and He, 2015). More importantly, we demonstrated  
402 unequivocally that FW2.2 is enriched at PD (**Figure 2**) and participates in cell-to-cell  
403 communication mechanisms via the regulation of PD permeability (**Figures 3**).

404 This localization at PD is most probably functionally conserved with other  
405 members of the CNR family. Indeed, the localization of the soybean GmFWL1 protein  
406 was described as associated to membrane microdomains (Qiao et al., 2017),  
407 according to a punctate pattern very similar to what we observed for FW2.2 in tomato  
408 (**Figure 2**). It is thus highly probable that GmFWL1 also localizes at PD. The closest  
409 homolog of FW2.2 in Arabidopsis, namely AtPRC2, belongs to the PD proteome  
410 established by Brault et al. (2019), together with well-established PD proteins, and  
411 presents a ~50- to 100-fold enrichment at PD compared to the PM, total protein,  
412 microsomal or cell wall fraction.

413 PD make the connection between adjacent cells to enable the diffusion of mobile  
414 signalling molecules (Wu and Gallagher, 2011). Using DANS assays, we  
415 demonstrated that FW2.2 is involved in cell-to-cell diffusion mechanisms and  
416 contributes to increase PD permeability (**Figure 3**). The permeability and thus the  
417 aperture of PD are mechanically regulated by the extent of deposited callose at the  
418 neck of PD (Amsbury et al., 2018). The increase in PD permeability mediated by  
419 FW2.2 occurs via a modification in the level of callose deposition, as FW2.2 regulates  
420 negatively its accumulation (**Figures 4-5**). The level of callose deposition is a highly  
421 regulated process involving two antagonistic enzymes, Callose Synthases and  $\beta$ -1,3-  
422 glucanases (Chen and Kim, 2009). Callose deposition is enhanced according to two  
423 main signalling pathways, one Reactive Oxygen Species (ROS)-dependent and the  
424 other one salicylic acid (SA)-dependent, which both induce the expression of receptor  
425 proteins such as PDLP5 that participate with Callose Synthase proteins in the  
426 regulation of PD permeability (Cui and Lee, 2016; Amsbury et al., 2018; Tee et al.,  
427 2022). The expected decrease in PD permeability under  $H_2O_2$  stress was not  
428 observed when FW2.2 is overexpressed, suggesting that FW2.2 play a role in the

429 ROS-dependent pathway. Whether FW2.2 plays also a role in the SA-dependent  
430 pathway to regulate PD permeability remains to be determined.

431

432 **FW2.2 interacts physically with Callose Synthases to modify their activity**

433 A proteomics approach using IP-MS/MS revealed that FW2.2 interacts with different  
434 Callose Synthases: SICalS1, SICalS3a, SICalS3b, SICalS9, SICalS10 and SICalS12  
435 (**Figure 6**). Interestingly, all these tomato proteins are the orthologs of Arabidopsis  
436 CalS known to contribute to callose homeostasis at PD, thereby regulating the  
437 permeability of PD and consequently the symplastic molecular exchanges between  
438 neighboring cells (Saatian et al., 2023; Usak et al., 2023). It is noteworthy that among  
439 the 178 proteins found to interact with GmFWL1, three distinct callose synthases,  
440 namely CalS5 (Glyma13g31310), CalS8 (Glyma04g36710) and CalS10  
441 (Glyma10g44150) were also identified following the co-immunoprecipitation assays  
442 (Qiao et al., 2017). This observation not only suggests that GmFWL1 is probably  
443 located at PD as well, but also that the interaction between FW2.2 and CNRs with  
444 proteins involved in the biosynthesis of callose and the metabolic process of callose  
445 deposition at PD seems to be a conserved feature for the balance between synthesis  
446 and degradation of callose at PD, and suggests that CNRs regulate negatively the  
447 activity of Callose Synthases.

448 CalS are very large proteins (more than 1900 aa) which possess multiple  
449 transmembrane spanning domains arranged in two regions delineating a cytoplasmic  
450 hydrophobic loop. This hydrophilic loop harbors the catalytic domain of the active  
451 CalS complex where UDP-Glucose transferase (UGT1) and Sucrose Synthase  
452 (Susy) may interact to provide substrates for callose synthesis (Verma and Hong,  
453 2001). As revealed by the topological analysis of FW2.2, the protein sequence  
454 between the two TMDs corresponds to a cytoplasmic/intracellular region (**Figure 1**).  
455 It is likely that this cytoplasmic region is involved in the interaction with CalS proteins  
456 and other putative interactors, as also shown for PfCNR1 (Li and He, 2017).

457 The activity of PD-associated Callose Synthases is of prime importance in  
458 numerous developmental processes, such as in response to biotic and abiotic stress,  
459 organ and tissue patterning, cell differentiation, phloem transport, and cell division via  
460 the formation of the cell plate at cytokinesis (Amsbury et al. 2018; Wu et al., 2018;  
461 Usak et al., 2023). In Arabidopsis, AtCalS1 and AtCalS10 localize at the nascent cell  
462 plate where they synthesize callose as the first and fundamental polysaccharide

463 component of the nascent cell plate, and AtCals9 is essential for the proper  
464 commitment to mitosis during male gametogenesis (Usak et al., 2023). Again,  
465 orthologs for these three Cals were found to interact with FW2.2 in tomato.  
466 Interestingly, the CRR1 protein from rice encodes a Cals which is essential for ovary  
467 growth following fertilization (Song et al., 2016). The loss-of-function of *CRR1*  
468 induces a disordered patterning of vascular cells in the ovaries of the mutant, with  
469 aberrant cell wall formation and reduced callose deposition at PD. Furthermore, the  
470 cell number inside the *crr1* ovaries is reduced when compared to the WT,  
471 establishing a link with callose synthesis and deposition, symplastic pathway via PD  
472 and control of cell division during ovary development.

473

474 **How to reconcile a function of FW2.2 in cell-to-cell communication, cell cycle-  
475 and fruit growth regulation?**

476 As FW2.2 was described as a negative regulator of cell division during early fruit  
477 development, which ultimately impacts fruit growth (Cong et al., 2002), it would have  
478 been expected that a loss-function of FW2.2 results in increased cell divisions and  
479 possibly larger organs (including fruits), and conversely that the ectopic  
480 overexpression of FW2.2 reduces mitotic activities and results in smaller organs. This  
481 latter effect could be observed at least in leaves from 35S::FW2.2 overexpressing  
482 lines (**Figure 3**), i.e. in organs where FW2.2 is not naturally expressed  
483 (**Supplemental Figure 2B**). Since the reduction in leaf growth was unrelated to any  
484 modification in cell size, this suggests that cell divisions were reduced under the  
485 effects of FW2.2 overexpression. In two out of three gain-of-function lines, we could  
486 also observe such a phenotype of reduced size for fruits although limited in extent  
487 (**Figure 5**).

488 These results are puzzling since genetics studies showed that the *fw2.2* QTL  
489 accounts for 22% to 47% of fruit mass variation when cultivated tomato cultivars are  
490 crossed with the wild species *Solanum pimpinellifolium* or *Solanum pennellii* (Alpert  
491 et al., 1995; Lippman and Tanksley, 2001; van der Knaap and Tanksley, 2003).  
492 Nevertheless, the literature is still devoid of any functional characterization of *FW2.2*  
493 in cultivated tomato plants, albeit the gene was discovered and cloned more than 20  
494 years ago. This is most probably the result of a lack of phenotypes when *FW2.2* is  
495 artificially deregulated in transgenic fruits. For instance, Zsögön et al. (2018) aimed at  
496 introducing by CRISPR-Cas9 engineering, yield and productivity traits from modern

497 ('large-fruited') tomato cultivars into the wild ('small-fruited') tomato *Solanum*  
498 *pimpinellifolium*. Among the six traits studied, these authors selected the *FW2.2* locus  
499 for fruit weight, and produced several mutants with deletions disrupting *FW2.2*.  
500 However, none of them induced any change in fruit size in T2 lines compared to *S.*  
501 *pimpinellifolium* WT, despite the mutations (Zsögön et al., 2018). These results  
502 corroborate the functional analysis reported herein in *S. lycopersicum* cv AC, when  
503 *FW2.2* was mutated in the *CR-fw2.2* loss-of-function plants (**Figure 5**). Hence, the  
504 ectopic and constitutive expression of *FW2.2* driven by the 35S promoter, definitely  
505 outside its natural timeframe and territorial regulation, and its loss of function did not  
506 impact fruit development, which probably obeys to precise changes in *FW2.2* spatio-  
507 temporal expression, according to the heterochronic regulation of expression  
508 described for the original *fw2.2* mutation (Cong et al., 2002). To cope with this  
509 difficulty, we developed an 'allele swapping' complementation strategy  
510 (**Supplemental Figure 8**). This strategy aimed at generating transgenic plants in  
511 which the 'large-fruit'-allele promoter from *S. lycopersicum* cv. AC is used to govern  
512 the expression of *FW2.2* in a 'small-fruit' background, namely the wild tomato *S.*  
513 *pimpinellifolium* (Pi). Conversely, we used the 'small-fruit'-allele promoter from *S.*  
514 *pimpinellifolium* to govern the expression of *FW2.2* in the 'large-fruit' AC background.  
515 Although we succeeded in the expected allele expression swapping according to the  
516 right spatio-temporal expression governed by each of the promoters, we failed to  
517 produce any fruit weight phenotypes in the complemented *S. pimpinellifolium* and *S.*  
518 *lycopersicum* cv. AC transgenic lines compared to WT plants. Therefore, the effects  
519 of *FW2.2* on fruit size obeys probably to a subtler regulation than the sole quantity of  
520 transcripts and availability of the protein. In addition, we cannot exclude that this lack  
521 of tangible phenotype may be related to gene redundancy within the *CNR/FWL*  
522 family, as 11 genes paralogous to *FW2.2* have been reported (Beauchet et al.,  
523 2021).

524 Despite the lack of consistent phenotypes when *FW2.2* is misexpressed, the  
525 functionality of the protein itself within its cellular and protein environment may be of  
526 prime importance. The discovery of the *FW2.2* function in cell-to-cell communication  
527 via PD thus raises the question of its link with the regulation of cell division, and  
528 subsequent fruit size control. By impairing callose deposition and thus maintaining  
529 PD aperture, *FW2.2* may contribute to facilitate the diffusion of signalling molecules  
530 whose nature is still unknown. As reviewed by Han et al. (2014b), TFs are well

531 characterized examples of such signalling molecules that could play an important  
532 part in the determination of fruit size. Recently, it was shown that a cold stress  
533 increases callose accumulation in the FM of tomato plants, resulting in impaired  
534 feedback loops which regulate the activity of WUSCHEL (WUS) (Wu et al., 2023).  
535 The TF WUS specifies the maintenance of stem cell activity in FM, and therefore a  
536 deregulation of WUS activity impacts the number of carpel primordia, and ultimately  
537 the number of locules inside the fruit. As a consequence of cold stress, *Ca/S* genes  
538 are induced and promote the callose deposition in the FM, which blocks the PD-  
539 mediated symplastic connection and alters the cell-to-cell movement of WUS which  
540 no longer can exert its negative regulatory action on *CLAVATA3* and *AGAMOUS*. As  
541 a result, the activity of *WUS* is not terminated in due time, which leads to increased  
542 cell divisions in the FM producing extra carpels and locules during fruit  
543 organogenesis (Wu et al., 2023). Interestingly, we observed similar trends in our  
544 transgenics plants: a higher number of locules resulting from increased cell divisions  
545 in FM in loss-of-function CR-fw2.2 lines, as callose deposition was increased, and the  
546 opposite effects in gain-of-function 35::FW2.2 lines (**Figure 5C**). FM termination  
547 requires the repression of WUS via a transcriptional repressor complex, involving the  
548 INHIBITOR OF MERISTEM ACTIVITY (IMA) protein (Bollier et al., 2018), which was  
549 described as a negative regulator of cell divisions. In particular, the overexpression of  
550 *IMA* leads to smaller fruits, while its repression enlarges the FM and leads to an  
551 increase in the locule number (Sicard et al., 2008). IMA and its transcriptional  
552 regulatory machinery may thus represent such signalling molecules whose diffusion  
553 across PD may be influenced by FW2.2 to determine fruit size, as *FW2.2* is  
554 expressed as early as in carpels of pre-anthesis floral buds (Frary et al., 2000), and  
555 preferentially expressed in the FM than in vegetative meristems (Park et al., 2012).

556 So far, direct evidences for the symplastic movements via PD of cell cycle  
557 regulators have not been reported. However, Weinl et al., (2005) showed that Cyclin-  
558 Dependent Kinase (CDK)-specific inhibitors called Kip-Related Proteins (KRPs) can  
559 act non-cell-autonomously, as to regulate cell division and growth pattern in leaf  
560 epidermis. During tomato fruit development, KRPs are key players in the regulation of  
561 cell cycle, and the commitment to endoreduplication which drives ploidy-dependent  
562 fruit growth (Bisbis et al., 2006; Nafati et al., 2011; Tourdot et al., 2023). Whether the  
563 negative regulation on cell division exerted by FW2.2 in fruit growth goes through the  
564 inactivation of CDK/Cyclin activities via the traffic of KRPs from cell to cell across the

565 pericarp remains an exciting matter of investigation. Recently, Ruan et al. (2020)  
566 reported that OsCNR1, encoded by the underlying gene of a major QTL for grain  
567 width and weight in rice, is able to interact with OsKRP1 in the cell membrane.  
568 Therefore, this remarkable finding provided the first evidence of a direct link between  
569 a CNR protein controlling organ size and a well-established cell cycle regulator  
570 inhibiting cell division. Whether this applies to FW2.2 for the regulation of cell cycle  
571 during early fruit development is a challenge for future research as to unravel  
572 definitely the function of FW2.2 in the control of fruit size/weight in tomato. Then, the  
573 lack of phenotypes observed in our in planta functional analysis may not be only  
574 related to the proper spatio-temporal expression of *FW2.2*, but also to the protein  
575 environment itself and the spatio-temporal availability of these putative signaling  
576 molecules.

577 How PD-mediated symplastic signalling affects fruit growth is still poorly  
578 understood. By demonstrating that FW2.2 contributes to the spatio-temporal  
579 regulation of callose deposition dynamics via regulating the CalS activity, we here  
580 provide an important breakthrough for the identification of the molecular and cellular  
581 mode of action of FW2.2. Based on our data, we propose a model integrating FW2.2  
582 in the regulation of PD aperture via the dynamics of callose deposition (**Figure 7**).  
583 We propose that FW2.2 interacts with CalS to regulate negatively its activity, thus  
584 impacting PD permeability and facilitating the cell-to-cell movement of mobile  
585 signalling molecules. A future challenge will be to identify the nature of such  
586 signalling molecules, which will provide a valuable insight into the molecular  
587 mechanisms underlying the complex regulation of organ size, especially fruits.

588

589

## 590 **METHODS**

### 591 **Plant materials and growth conditions**

592 Tomato (*Solanum lycopersicum* cv. AC) and tobacco (*Nicotiana benthamiana*) plants  
593 were grown in soil in a greenhouse under the following conditions: 16 h day/8 h night  
594 cycle, using a set of 100 W warm white LED projectors providing an irradiance of 100  
595  $\mu\text{mol m}^{-2} \text{s}^{-1}$  at the level of canopy. The light spectrum was constituted by equivalent  
596 levels of blue irradiation (range 430–450 nm) and red irradiation (640–660nm). For in  
597 vitro culture, tomato seeds were sterilized for 10 min under agitation in a solution of  
598 3.2% bleach. Seeds were then washed three times with sterile water and dried under

599 a laminar flow hood. Seeds were sowed in Murashige and Skoog medium (1/4 MS)  
600 and transferred in a growth chamber under the following conditions: 16 h day/8 h  
601 night cycle, 22°C/20°C day/night, using white light (Osram L36 W/77 Fluora 1400 lm)  
602 providing 80 to 100  $\mu$ E m<sup>-2</sup> s<sup>-1</sup> intensity light at the stirring plate.

603

604 **Vector constructs and plant transformation**

605 Vectors for the overexpression of *FW2.2* in plants were generated using the  
606 Gateway® cloning system (Invitrogen, Carlsbad, CA, USA), following manufacturer's  
607 instruction. The *FW2.2* full-length coding sequence was amplified from cDNAs  
608 prepared from tomato (cv. AC) fruits at 5 DPA using PrimeSTAR MAX DNA  
609 polymerase (TAKARA BIO Inc., Kusatsu, Japan) and primers including the attB sites  
610 (**Supplemental Table 1**). The resulting PCR products were cloned into the  
611 corresponding Gateway vectors described in **Supplemental Table 2**. For  
612 CRISPR/Cas9 mutagenesis, constructs were assembled using the Golden Gate  
613 cloning method (Weber et al., 2011). Two sgRNAs were designed at the 5' end of the  
614 coding sequence of *FW2.2* using CRISPOR (Concordet and Haeussler, 2018) to  
615 generate a premature stop codon (**Supplemental Table 1**). Primers for creating the  
616 sgRNA were designed as follows: tgtggtctcaATTG-NNNNNNNN-  
617 gtttagagctagaaatagcaag as a forward primer containing the sgRNA, and  
618 tgtggtctCAAGCGTAATGCCAACTTTGTAC as a reverse primer. The sequences  
619 corresponding to the sgRNA were then PCR amplified using the two aforementioned  
620 primers, and cloned into the pSLQ1651-sgTelomere plasmid (Addgene #51024).  
621 *fw2.2*-sgRNA-1 and *fw2.2*-sgRNA-2 were fused to the *Arabidopsis* AtU6-26 promoter  
622 (Addgene #46968) by digestion-ligation reaction in pLCH47751 (Addgene #48002)  
623 and pLCH47761 (Addgene #48003) respectively. These two level 1 vectors were  
624 assembled with the Kanamycin resistance gene (pNOS::NPTII-OCST; Addgene  
625 #51144), the AtCas9 (2x35S::AtCAS9-OCST; Addgene #112079) and the linker  
626 pLCH41780 (Addgene #48019) into the level 2 vector pICSL4723 (Kind gift from Dr  
627 Mark Youles, The Sainsbury Laboratory, Norwich, UK). Transgenic plants were  
628 generated by *Agrobacterium tumefaciens* (strain C58C1) mediated transformation  
629 using explants of tomato cotyledons as described (Swinnen et al., 2022).

630

631 **RNA extraction and RT-qPCR analysis**

632 Total RNA was isolated from cotyledons, hypocotyls, shoot apical meristems, leaves,  
633 roots, flowers and pericarp tissues from fruits harvested at different developmental  
634 stages (5, 10, and 15 DPA), using TRIzol reagent (Invitrogen) in combination with  
635 RNeasy Plant Mini Kit (Qiagen) following the manufacturers' instructions. RNase-free  
636 DNase (Qiagen) treatment was performed on each sample. Reverse transcription  
637 was performed using the iScript<sup>TM</sup> cDNA Synthesis Kit (Bio-Rad, Hercules, CA).  
638 Real-time PCR was performed using Gotaq<sup>®</sup> qPCR mastermix (Promega, Madison,  
639 WI) and a CFX 96 real-time system (Bio-Rad). qPCR primers were designed with  
640 PerlPrimer software (Marshall, 2004) to overlap 2 exons in order to limit genomic  
641 DNA amplification (**Supplemental Table 1**) and amplify a 80 to 200 bp-long  
642 amplicon, with a Tm of 60°C. The transcript levels of the expressed genes were  
643 normalized to that of the housekeeping genes: *SITUBULIN* (Solyc04g081490) in  
644 combination with *SINUDK* (Solyc01g089970) for fruit samples, or with *SEIF4a*  
645 (Solyc12g095990) for other tissue samples.

646

#### 647 **Phenotypic characterization**

648 Plants were cultivated randomly side-by-side with WT plants. Flowers were vibrated  
649 every day to ensure optimal self-pollination. Seven flowers per inflorescence were  
650 maintained to ensure proper development of fruit per inflorescence. Fruits from four  
651 to six plants of each genotype of two biological replicates were used to determine  
652 fruit weight, fruit size, locule number and pericarp thickness at the breaker stage of  
653 fruit development. Fruits were weighted and measured using a caliper. Then, pictures  
654 of equatorial transverse sections of fruits were taken to count the locule number and  
655 measure the pericarp thickness, using a Nikon D5300 camera. Image analysis was  
656 performed using the ImageJ software (<https://imagej.nih.gov/ij/>). The number of  
657 measurements ranged from n= 50 to n= 200 depending on the number of fruits  
658 produced by the different transgenic plants. For leaf surface phenotyping, pictures of  
659 full grown leaves were taken using a Nikon D5300 and analysed by intensity  
660 threshold filtering. To measure the leaf thickness, images of leaf sections acquired for  
661 immuno-labelling experiments were used with three measurement for each picture  
662 (n=70 to 100).

663

#### 664 **PD index determination**

665 The localization of FW2.2-YFP at PM and PD was observed using confocal imaging  
666 performed on a Zeiss LSM 880 confocal laser scanning microscope equipped with  
667 fast AiryScan, using a Zeiss C PL APO x63 oil-immersion objective (numerical  
668 aperture 1.4). Staining with FM4.64 at a final concentration of 4  $\mu$ M was used as a  
669 control for PM localization (Bolte et al., 2004). For FM4.64 imaging, excitation was  
670 performed at 561 nm and fluorescence emission was collected at 630-690 nm. For  
671 YFP imaging, excitation was performed at 514 nm and fluorescence emission  
672 collected at 520-580 nm. Staining with aniline blue (Biosupplies, Victoria, Australia)  
673 was performed by infiltration of a 0.0125% solution; excitation was performed at 405  
674 nm and fluorescence emission collected at 420-480 nm. The calculation of PD index  
675 was determined by calculating the fluorescence intensity of FW2.2-YFP at  
676 plasmodesmata and at PM as described (Grison et al., 2019). Images were all  
677 acquired with the same parameters (zoom, gain, laser intensity, etc.), and YFP and  
678 AB channels were acquired sequentially. Ten to twenty images were acquired with a  
679 minimum of three biological replicates. Individual images were processed using  
680 ImageJ. A minimum of ten regions of interest (ROI) at PD (using AB as a marker) and  
681 in the surrounding PM were manually outlined, and the signal intensity was  
682 calculated as the mean gray value (sum of gray values of all the pixels in the selected  
683 area divided by the ROI surface) for each ROI.

684

#### 685 **Immuno-labelling of callose**

686 The level of callose deposition was determined in leaves and in the pericarp of fruits  
687 harvested at 5 and 15 DPA. Leaf fragments were fixed with a 4% formaldehyde  
688 solution in 1X PBS for 30 min, using vacuum infiltration (~100 kPa). They were then  
689 embedded in 6% SeaKem® LE agarose (Lonza, Basel, Switzerland), and sections of  
690 100  $\mu$ m were realized using a vibrating blade microtome (Microm 650V; Thermo  
691 Fischer Scientific, Walldorf, Germany). Equatorial pericarp fragments were fixed  
692 using the same protocol. Pericarp sections of 80 or 150  $\mu$ m were prepared, and fixed  
693 once more in fresh formaldehyde solution for 30 min, rinsed and kept in 1X PBS until  
694 use. The leaf and pericarp sections were then processed using the same protocol.  
695 The sections were deposited into a small basket containing MTSB buffer (50 mM  
696 PIPES, 5 mM EGTA, 5 mM MgSO<sub>4</sub>, pH=7) to perform the immuno-labelling of callose  
697 using the InsituPro VSi automated immunohistochemistry device from Intavis (Köln,  
698 Germany). Leaf and pericarp sections were rinsed 4 times for 10 min with 700  $\mu$ L of

699 MTSB. The sections were then incubated for 1 h with 700  $\mu$ L of a 10% (v/v)  
700 DMSO/3% (v/v) IGEPAL<sup>®</sup> CA-630 (Merck, Darmstadt, Germany) in MTSB. After  
701 rinsing, pericarp sections were incubated for 2 h in a 5% (v/v) Normal Donkey serum  
702 (NDS; Merck) blocking solution in MTSB, and 4 h with 700  $\mu$ L of a 1/250 dilution of  
703 Anti-callose primary antibody (Biosupplies) in MTSB supplemented with 5% (v/v)  
704 NDS. The sections were then washed 6 times with 700  $\mu$ L of MTSB, and incubated  
705 for 2 h with 700  $\mu$ L of a 1/250 dilution of anti-mouse IgG Alexa Fluor<sup>TM</sup> 555 secondary  
706 antibody (ab150106; Abcam, Cambridge, UK) in MTSB + 5% (v/v) NDS. Sections  
707 were rinsed 6 times in MTSB and incubated with 1  $\mu$ g/mL Calcofluor white  
708 (Fluorescent Brightener 28 disodium salt solution, Merck, in MTSB). After rinsing, the  
709 sections were mounted on glass slides with citifluor (AF1-25) (EMS Acquisition Corp.,  
710 PA, USA) and the slides sealed with nail polish.

711 Identical confocal microscope acquisition parameters were used for all the  
712 samples. Because of the highly heterogeneous cellular structure of pericarp and leaf,  
713 the total signal intensity of each tissue was quantified, and signal intensity values  
714 were measured by integrating the gray value of all the pixels above the same  
715 threshold. A minimum of six measurements was performed at least on 5 sections  
716 from at least three different fruits or leaves from different plants, and the experiment  
717 was repeated twice.

718 During the callose immuno-labelling experiments, leaf thickness, cell perimeter in  
719 leaves or fruits have been manually measured following staining with Calcofluor on  
720 pictures acquired from confocal microscopy using ImageJ.

721

## 722 **DANS assays**

723 Before proceeding the DANS assay, 4-week-old tomato plants were pre-treated by  
724 spraying water (mock) or 10 mM H<sub>2</sub>O<sub>2</sub>, followed by a 2 h incubation. Then eight  
725 droplets (~1 $\mu$ L) of 1mM CFDA (Merck, Darmstadt, Germany) per leaf sample were  
726 loaded on the upper (adaxial) surface. Then, the diffusion of the dye was monitored  
727 on the lower (abaxial) surface of the leaf, 5 min after loading CFDA, using an  
728 Axiozoom stereomicroscope V16 (Carl Zeiss Microscopy) equipped with a Zeiss  
729 Plan-Neofluar 0.5x (NA 0.19) objective lens, a fluorescence lamp (Lumencor Sola  
730 LED) and a GFP-BP filter cube. Several leaves with the same size were used from at  
731 least 4-5 plants (n=100). Imaging was performed at the same magnification, laser  
732 power and gain and pictures were acquired using a CMOS Axiocam 105 color

733 camera. The CF signal intensity was measured on ImageJ by integrating the signal  
734 intensity to the pixel surface.

735

736 **Co-immunoprecipitation and mass-spectrometry analysis**

737 Total protein extracts from 100 mg of 35S::FW2.2-YFP fruit pericarp tissue were  
738 prepared using the following buffer: 1X PBS, cOmplete Protease Inhibitor Cocktail  
739 tablets (Roche, Mannheim, Germany) and 1% Triton X-100. Samples were incubated  
740 in the extraction buffer at 4°C for 30 min with agitation, and then centrifuged (16000g,  
741 10 min, 4 °C). The supernatant containing the resuspended proteins was used for  
742 immunoprecipitation assay using anti-GFP microbeads provided in the μMACS  
743 Epitope Tag Protein Isolation Kit according to the manufacturer's protocol (Miltenyi  
744 Biotec, Bergisch Gladbach, Germany). Approximately, 500 µg of soluble proteins  
745 were loaded for each co-IP assay.

746 Fifty µL of the resulting eluate was loaded on a 10% SDS-PAGE acrylamide gel;  
747 gel bands were manually cut and transferred to 1.5 mL Eppendorf tubes. Bands were  
748 first washed with 500 µL of water and then 500 µL of 25 mM NH<sub>4</sub>HCO<sub>3</sub>. Destaining  
749 was performed twice in the presence of 500 µL of 50 % acetonitrile (ACN) in 25 mM  
750 NH<sub>4</sub>HCO<sub>3</sub>. Gel bands were dehydrated twice by 500 µL of 100 % ACN, and finally  
751 dried at room temperature. Following destaining, proteins were reduced with 500 µL  
752 of 10 mM DTT at 56°C for 45 min. The supernatant was then removed and proteins  
753 were alkylated with 500 µL of 55 mM iodoacetamide for 30 min. Gel bands were  
754 washed twice with 500 µL of 50 % ACN in 25 mM NH<sub>4</sub>HCO<sub>3</sub>, then dehydrated by 500  
755 µL of 100 % CH<sub>3</sub>CN, and finally dried at room temperature. Twenty microliters of a  
756 trypsin solution (Sequencing Grade Modified Trypsin, Promega, Madison, USA), at a  
757 concentration of 0.0125 µg/µL in 25 mM NH<sub>4</sub>HCO<sub>3</sub>, was added to every gel region  
758 and gel bands were kept for 10 min on ice. Fifty microliters of 25 mM NH<sub>4</sub>HCO<sub>3</sub> were  
759 added, and the samples were kept for another 10 min at room temperature. The  
760 digestion was performed overnight at 37°C; then peptides were extracted by addition  
761 100 µL of 2% formic acid (FA). Gel bands were extracted twice by addition of 200 µL  
762 of 80% ACN and 2% FA. After solvent evaporation in a Speed-vac, peptides were  
763 resuspended in 10 µL of 2% FA, then purified with a micro tip C18 (Zip-Tip C18  
764 Millipore Corporation Billerica MA, USA). Peptides were eluted with a solution  
765 containing 2% FA (v/v) and 80% ACN (v/v) and dried until total evaporation. Peptides  
766 were resuspended in 7 µL 2% FA before LC-MS/MS analysis.

767 The LC-MS/MS were performed using the Ultimate 3000 RSLC nano system  
768 (Thermo Fisher Scientific Inc, Waltham, MA, USA) interfaced online with a nano easy  
769 ion source and the Exploris 240 Plus Orbitrap mass spectrometer (Thermo Fisher  
770 Scientific Inc, Waltham, MA, USA). The samples were analysed in Data Dependent  
771 Acquisition (DDA). The raw files were analysed with MaxQuant version 2.0.3 using  
772 default settings. The files were searched against the *Solanum lycopersicum* genome  
773 (ITAG4.1\_release January 2022  
774 [https://solgenomics.net/organism/solanum\\_lycopersicum/genome](https://solgenomics.net/organism/solanum_lycopersicum/genome) 34689 entries)  
775 added with the FW2.2-YFP. Identified proteins were filtered according to the following  
776 criteria: at least two different trypsin peptides with at least one unique peptide, an E  
777 value below 0.01 and a protein E value smaller than 0.01 were required. Using the  
778 above criteria, the rate of false peptide sequence assignment and false protein  
779 identification were lower than 1%. Proteins were quantified by label-free method with  
780 MaxQuant software using unique and razor peptides intensities (Cox et al., 2014).  
781 Statistical analyses were carried out using RStudio package software. The protein  
782 intensity ratio and statistical tests were applied to identify the significant differences in  
783 the protein abundance. Hits were retained if they were quantified in at least four of  
784 the five replicates in at least one experiment. Proteins with a significant quantitative  
785 ratio ( $P < 0.05$  or 0.01 with or without Benjamini correction) were considered as  
786 significantly up-regulated and down-regulated respectively.

787

## 788 **Supplemental Data**

789 **Supplemental Figure 1.** Characterization of plants expressing FW2.2 fused to YFP.

790 **Supplemental Figure 2.** RT-qPCR analysis of FW2.2 expression in tomato plants.

791 **Supplemental Figure 3.** CRISPR/Cas9-induced mutations producing truncated  
792 versions of FW2.2/CNR lacking the PLAC8 domain.

793 **Supplemental Figure 4.** DANS assays in tomato leaves.

794 **Supplemental Figure 5.** Pericarp cell perimeter in the different transgenic lines.

795 **Supplemental Figure 6.** Characterization of Callose Synthase genes in tomato.

796 **Supplemental Figure 7.** Ca/S expression level in leaves and fruit from WT,  
797 35S::FW2.2 and CR-FW2.2 lines.

798 **Supplemental Figure 8.** Allele swapping complementation assays.

799 **Supplemental Table 1.** List of primers used for constructs and RT-qPCR analysis.

800 **Supplemental Table 2.** List of Gateway vectors used for constructs.

801 **Supplemental Data Set 1.** List of proteins identified as interactors of FW2.2/CNR.

802

803 **Acknowledgements**

804 This work was carried out with the financial support of the French Agence Nationale  
805 de la Recherche (grant no. ANR-20-CE20-0002), the GPR Bordeaux Plant Sciences  
806 in the framework of the IdEX Bordeaux University ‘Investments for the Future’  
807 program, and the French Ministère de l’Enseignement Supérieur et de la Recherche  
808 (PhD grant to A. Beauchet). Mass spectrometry experiments were carried out using  
809 the facilities of the Montpellier Proteomics Platform (PPM, BioCampus Montpellier,  
810 France). The microscopy analyses were performed in the Bordeaux Imaging Center,  
811 a service unit of the CNRS-INSERM and Bordeaux University, member of the  
812 national infrastructure France BioImaging, and supported by the French National  
813 Research Agency (ANR-10-INBS-04). The help of Lysiane Brocard is acknowledged.  
814 We express our deepest thanks to Isabelle Atienza, Aurélie Honoré and Valérie  
815 Rouyère, for taking care of the plant culture in the greenhouse.

816

817 **Author contribution**

818 N.B., F.G., E.B., N.G. and C.C. conceived the project and designed the research.  
819 A.B. and N.B. performed the research. V.R. performed the IP-MS-MS proteomics  
820 experiments. M.G. helped in the callose immuno-labelling experiments using the  
821 InsituPro VSi automate. All authors analyzed and discussed the results. A.B., N.B.,  
822 N.G. and C.C. wrote the manuscript with input from the other authors.

823

824 **Conflict of interest**

825 The authors declare that they have no conflicts of interest.

826

827

828 **References**

829 Alpert, K. B., Grandillo, S. and Tanksley, S. D. (1995). *fw2.2*: a major QTL controlling  
830 fruit weight is common to both red- and green-fruited tomato species. *Theor. Appl.*  
831 *Genet.* 91: 994–1000.

832 Amsbury, S., Kirk, P. and Benitez-Alfonso, Y. (2018). Emerging models on the  
833 regulation of intercellular transport by plasmodesmata-associated callose. *J. Exp.*  
834 *Bot.* 69: 105–115.

835 Baldet, P., Hernould, M., Laporte, F., Mounet, F., Just, D., Mouras, A., Chevalier, C.  
836 and Rothan C. (2006). The expression of cell proliferation-related genes in early  
837 developing flower is affected by fruit load reduction in tomato plants. *J. Exp. Bot.*  
838 57: 961-970

839 Beauchet, A., Gévaudant, F., Gonzalez, N. and Chevalier, C. (2021). In search of the  
840 still unknown function of FW2.2/CELL NUMBER REGULATOR, a major regulator  
841 of fruit size in tomato. *J. Exp. Bot.* 72: 5300–5311.

842 Bisbis, B., Delmas, F., Joubès, J., Sicard, A., Hernould, M., Inzé, D., Mouras, A. and  
843 Chevalier, C. (2006). Cyclin-Dependent Kinase Inhibitors are involved in  
844 endoreduplication during tomato fruit development. *J. Biol. Chem.* 281: 7374-7383.

845 Blanca, J., et al. (2015). Genomic variation in tomato, from wild ancestors to  
846 contemporary breeding accessions. *BMC Genomics* 16: 257.

847 Bollier, N. et al. (2018). At-MINI ZINC FINGER2 and SI-INHIBITOR OF MERISTEM  
848 ACTIVITY, a conserved missing link in the regulation of floral meristem termination  
849 in *Arabidopsis* and Tomato. *Plant Cell* 30: 83-100

850 Bolte, S. et al. (2004). FM-dyes as experimental probes for dissecting vesicle  
851 trafficking in living plant cells. *J. Microsc.* 214: 159–173.

852 Brandizzi F., et al. (2002). The destination for single-pass membrane proteins is  
853 influenced markedly by the length of the hydrophobic domain. *Plant Cell* 14: 1077–  
854 1092.

855 Brault, M.L. et al. (2019). Multiple C2 domains and transmembrane region proteins  
856 (MCTPs) tether membranes at plasmodesmata. *EMBO Rep.* 20: e47182.

857 Chakrabarti, M. et al. (2013). A cytochrome P450 regulates a domestication trait in  
858 cultivated tomato. *Proc. Natl. Acad. Sci. USA* 110: 17125–17130.

859 Chen, X.Y. and Kim, J.Y. (2009). Callose synthesis in higher plants. *Plant Signal.*  
860 *Behav.* 4: 489–492.

861 Concordet, J.-P. and Haeussler, M. (2018). CRISPOR: intuitive guide selection for  
862 CRISPR/Cas9 genome editing experiments and screens. *Nucleic Acids Res.* 46:  
863 W242–W245.

864 Cong, B., Liu, J. and Tanksley, S. D. (2002). Natural alleles at a tomato fruit size  
865 quantitative trait locus differ by heterochronic regulatory mutations. *Proc. Natl.*  
866 *Acad. Sci. USA* 99: 13606–13611.

867 Cong, B. and Tanksley, S. D. (2006). FW2.2 and cell cycle control in developing  
868 tomato fruit: a possible example of gene co-option in the evolution of a novel  
869 organ. *Plant Mol. Biol.* 62: 867–880.

870 Cox, J., Hein, M.Y., Luber, C.A., Paron, I., Nagaraj, N. and Mann, M. (2014).  
871 Accurate proteome-wide label-free quantification by delayed normalization and  
872 maximal peptide ratio extraction, termed MaxLFQ. *Mol Cell Proteomics* 13: 2513-  
873 2526.

874 Cui, W. and Lee, J.-Y. (2016). Arabidopsis callose synthases CalS1/8 regulate  
875 plasmodesmal permeability during stress. *Nat. Plants* 2: 16034.

876 Cui, W., Wang, X. and Lee, J.-Y. (2015). Drop-ANd-See: A Simple, Real-Time, and  
877 Noninvasive Technique for Assaying Plasmodesmal Permeability. In  
878 *Plasmodesmata: Methods and Protocols*, M. Heinlein, ed, *Methods in Molecular*  
879 *Biology* (Springer: New York, NY), pp. 149–156.

880 Dahan, Y., Rosenfeld, R., Zadiranov, V. and Irihimovitch, V. (2010). A proposed  
881 conserved role for an avocado FW2.2-like gene as a negative regulator of fruit cell  
882 division. *Planta* 232: 663–676 .

883 De Franceschi, P. et al. (2013). Cell number regulator genes in *Prunus* provide  
884 candidate genes for the control of fruit size in sweet and sour cherry. *Molecular*  
885 *Breeding* 32: 311–326.

886 Doganlar, S., Frary, A., Daunay, M.-C., Lester, R.N. and Tanksley, S.D. (2002).  
887 Conservation of gene function in the Solanaceae as revealed by comparative  
888 mapping of domestication traits in Eggplant. *Genetics* 161: 1713–1726.

889 Frary, A. et al. (2000) .fw2.2: A Quantitative Trait Locus Key to the Evolution of  
890 Tomato Fruit Size. *Science* 289: 85–88.

891 Galaviz-Hernandez, C. et al. (2003). Plac8 and Plac9, novel placental-enriched  
892 genes identified through microarray analysis. *Gene* 309: 81–89.

893 Gallagher, K. L., Sozzani, R. and Lee, C.-M. (2014). Intercellular Protein  
894 Movement: Deciphering the Language of Development. *Annu. Rev. Cell Dev. Biol.*  
895 30: 207–233.

896 Gaudioso-Pedraza, R. et al. (2018). Callose-Regulated Symplastic Communication  
897 Coordinates Symbiotic Root Nodule Development. *Curr. Biol.* 28: 3562-3577.

898 Grandillo, S., Ku, H. M. and Tanksley, S. D. (1999). Identifying the loci responsible for  
899 natural variation in fruit size and shape in tomato. *Theor. Appl. Genet.* 99: 978–  
900 987.

901 Grison, M. S. et al. (2019). Plasma Membrane-Associated Receptor-like Kinases  
902 Relocalize to Plasmodesmata in Response to Osmotic Stress. *Plant Physiol.* 181:  
903 142–160.

904 Guo, M. et al. (2010). *Cell Number Regulator1* Affects Plant and Organ Size in  
905 Maize: Implications for Crop Yield Enhancement and Heterosis. *Plant Cell* 22:  
906 1057–1073.

907 Han, X. et al. (2014a). Auxin-Callose-Mediated Plasmodesmal Gating Is Essential for  
908 Tropic Auxin Gradient Formation and Signaling. *Dev. Cell* 28: 132–146.

909 Han, X. et al. (2014b). Transcription factor-mediated cell-to-cell signalling in plants. *J.*  
910 *Exp. Bot.* 65: 1737–1749.

911 Lemoine, F., Correia, D., Lefort, V., Doppelt-Azeroual, O., Mareuil, F., Cohen-  
912 Boulakia, S. and Gascuel, O. (2019). NGPhylogeny.fr: new generation  
913 phylogenetic services for non-specialists. *Nucleic Acids Res.* 47: W260-W265.

914 Li, Z. and He, C. (2015). *Physalis floridana* Cell Number Regulator1 encodes a cell  
915 membrane-anchored modulator of cell cycle and negatively controls fruit size. *J.*  
916 *Exp. Bot.* 66: 257–270.

917 Libault, M. et al. (2010). A member of the highly conserved FWL (tomato FW2.2-like)  
918 gene family is essential for soybean nodule organogenesis: A soybean FWL  
919 essential for nodulation. *Plant J.* 62: 852–864.

920 Lippman, Z. B. and Tanksley, S.D. (2001). Dissecting the Genetic Pathway to  
921 Extreme Fruit Size in Tomato Using a Cross Between the Small-Fruited Wild  
922 Species *Lycopersicon pimpinellifolium* and *L. esculentum* var. Giant Heirloom.  
923 *Genetics* 158: 413–422.

924 Liu, J., Cong, B. and Tanksley, S.D. (2003). Generation and analysis of an artificial  
925 gene dosage series in tomato to study the mechanisms by which the cloned  
926 quantitative trait locus fw2.2 controls fruit size. *Plant Physiol.* 132: 292–299.

927 Marshall, O.J. (2004). PerlPrimer: cross-platform, graphical primer design for  
928 standard, bisulphite and real-time PCR. *Bioinformatics* 20: 2471–2472.

929 Martiniere, A. et al. (2012). Cell wall constrains lateral diffusion of plant plasma-  
930 membrane proteins. *Proc. Natl. Acad. Sci. USA* 109: 12805–12810.

931 Martinière, A., Gibrat, R., Sentenac, H., Dumont, X., Gaillard, I., and Paris, N. (2018).  
932 Uncovering pH at both sides of the root plasma membrane interface using  
933 noninvasive imaging. *Proc. Natl. Acad. Sci. USA* 115: 6488–6493.

934 Maule, A. J., Benitez-Alfonso, Y. and Faulkner, C. (2011). Plasmodesmata –  
935 membrane tunnels with attitude. *Curr. Opin. Plant Biol.* 14: 683–690.

936 Mu, Q. et al. (2017). Fruit weight is controlled by Cell Size Regulator encoding a  
937 novel protein that is expressed in maturing tomato fruits. *PLOS Genet.* 13:  
938 e1006930.

939 Nafati, M., Cheniclet, C., Hernould, M., Do, P.T., Fernie, A., Chevalier, C. and  
940 Gévaudant F. (2011). The specific overexpression of a Cyclin Dependent Kinase  
941 Inhibitor in tomato fruit mesocarp cells uncouples endoreduplication and cell  
942 growth. *Plant J.* 65: 543–556.

943 Nesbitt, T.C. and Tanksley, S.D. (2001). fw2.2 Directly Affects the Size of Developing  
944 Tomato Fruit, with Secondary Effects on Fruit Number and Photosynthate  
945 Distribution. *Plant Physiol.* 127: 575–583.

946 O'Lexy, R. et al. (2018). Exposure to heavy metal stress triggers changes in  
947 plasmodesmatal permeability via deposition and breakdown of callose. *J. Exp.*  
948 *Bot.* 69, 3715–3728.

949 Park, S.J., Jiang, K., Schatz, M. C. and Lippman, Z. B. (2012). Rate of meristem  
950 maturation determines inflorescence architecture in tomato. *Proc. Natl. Acad. Sci.*  
951 *USA* 109: 639–644.

952 Petit, J. D., Li, Z. P., Nicolas, W. J., Grison, M. S. and Bayer, E. M. (2020). Dare to  
953 change, the dynamics behind plasmodesmata-mediated cell-to-cell  
954 communication. *Curr. Opin. Plant Biol.* 53: 80–89.

955 Platre, M.P., et al. (2022). The receptor kinase SRF3 coordinates iron-level and  
956 flagellin dependent defense and growth responses in plants. *Nat Commun.* 13:  
957 4445.

958 Qiao, Z. et al. (2017). The Gm *FWL1* (*FW2-2-like*) nodulation gene encodes a  
959 plasma membrane microdomain-associated protein: A FW2-2-like protein is  
located in plasma membrane microdomains. *Plant Cell Environ.* 40: 1442–1455.

Ruan, B. et al. (2020). Natural variation in the promoter of TGW2 determines grain  
width and weight in rice. *New Phytol.* 227: 629–640.

Saatian, B., Kolhalmi S.E. and Cui, Y. (2023). Localization of *Arabidopsis* Glucan

960       Synthase-Like 5, 8, and 12 to plasmodesmata and the GSL8-dependent role of  
961       PDLP5 in regulating plasmodesmal permeability. *Plant Signaling Behav.* 18:  
962       e2164670.

963       Sicard, A., Petit, J., Mouras, A., Chevalier, C. and Hernould, M. (2008). Meristem  
964       activity during flower and ovule development in tomato is controlled by the mini  
965       zinc finger gene *INHIBITOR OF MERISTEM ACTIVITY*. *Plant J.* 55: 415-427.

966       Song, W.-Y. et al. (2004). A Novel Family of Cys-Rich Membrane Proteins Mediates  
967       Cadmium Resistance in Arabidopsis. *Plant Physiol.* 135: 1027–1039.

968       Song, W.-Y. et al. (2010). *Arabidopsis* PCR2 Is a Zinc Exporter Involved in Both Zinc  
969       Extrusion and Long-Distance Zinc Transport. *Plant Cell* 22: 2237–2252.

970       Song L., Wang, R., Zhang, L., Wang, Y. and Yao, S. (2016). CRR1 encoding callose  
971       synthase functions in ovary expansion by affecting vascular cell patterning in rice.  
972       *Plant J.* 88: 620–632.

973       Swinnen, G., et al. (2022) SIKIX8 and SIKIX9 are negative regulators of leaf and fruit  
974       growth in tomato. *Plant Physiol.* 188: 382-396.

975       Tee, E. E., Johnston, M. G., Papp, D. and Faulkner, C. (2022). A PDLP-NHL3  
976       complex integrates plasmodesmal immune signaling cascades. *Proc. Natl. Acad.*  
977       *Sci. USA* 120: e2216397120.

978       Thomas, C.L., Bayer, E.M., Ritzenhaler, C., Fernandez-Calvino, L., and Maule, A.J.  
979       (2008). Specific targeting of a plasmodesmal protein affecting cell-to-cell  
980       communication. *PLoS Biol.* 6: e7.

981       Tourdot, E., Mauxion, J.-P., Gonzalez, N. and Chevalier C. (2023). Endoreduplication  
982       in plant organogenesis: a means to boost fruit growth. *J. Exp. Bot.* erad235,  
983       <https://doi.org/10.1093/jxb/erad235>.

984       Usak, D., Haluska, S. and Pleskot, R. (2023). Callose synthesis at the center point of  
985       plant development - An evolutionary insight. *Plant Physiol.* kiad274,  
986       <https://doi.org/10.1093/plphys/kiad274>

987       van der Knaap, E. and Tanksley, S. D. (2003). The making of a bell pepper-shaped  
988       tomato fruit: identification of loci controlling fruit morphology in Yellow Stuffer  
989       tomato. *Theor. Appl. Genet.* 107: 139–147.

990       Van Norman, J. M., Breakfield, N. W. and Benfey, P. N. (2011). Intercellular  
991       Communication during Plant Development. *Plant Cell* 23: 855–864.

992 Verma, D. P. S. and Hong Z. (2001). Plant callose synthase complexes. *Plant Mol.*  
993 *Biol.* 47: 693-701.

994 Wang, Y., et al. (2023). Plasmodesmata mediate cell-to-cell transport of  
995 brassinosteroid hormones. *Nat. Chem. Biol.* In press.

996 Weber, E., Gruetzner, R., Werner, S., Engler, C. and Marillonnet, S. (2011).  
997 Assembly of Designer TAL Effectors by Golden Gate Cloning. *PLoS ONE* 6:  
998 e19722.

999 Wei, Z., Wang, J., Yang, S. and Song, Y. (2015). Identification and expression  
1000 analysis of the LRR-RLK gene family in tomato (*Solanum lycopersicum*) Heinz  
1001 1706. *Genome* 58: 121–134.

1002 Weinl, C. et al. (2005). Novel Functions of Plant Cyclin-Dependent Kinase Inhibitors,  
1003 ICK1/KRP1, Can Act Non-Cell-Autonomously and Inhibit Entry into Mitosis. *Plant*  
1004 *Cell* 17: 1704–1722.

1005 Wu, J. et al. (2023). Cold stress induces malformed tomato fruits by breaking the  
1006 feedback loops of stem cell regulation in floral meristem. *New Phytol.* 237: 2268–  
1007 2283.

1008 Wu, S. and Gallagher, K.L. (2011). Mobile protein signals in plant development. *Curr.*  
1009 *Opin. Plant Biol.* 14: 563–570

1010 Wu, S.-W., Kumar, R., Iswanto, A.B.B. and Kim, J.-Y. (2018). Callose balancing at  
1011 plasmodesmata. *J. Exp. Bot.* 69: 5325–5339.

1012 Xie, W., Nielsen, M.E., Pedersen, C., and Thordal-Christensen, H. (2017). A Split-  
1013 GFP Gateway cloning system for topology analyses of membrane proteins in  
1014 plants. *PLoS ONE* 12: e0170118.

1015 Xu, J. et al. (2013). Molecular characterization and functional analysis of “fruit-  
1016 weight2.2-like” gene family in rice. *Planta* 238: 643–655.

1017 Yan, D. et al. (2019). Sphingolipid biosynthesis modulates plasmodesmal  
1018 ultrastructure and phloem unloading. *Nat. Plants* 5: 604–615.

1019 Zsögön, A. et al. (2018). De novo domestication of wild tomato using genome editing.  
1020 *Nat. Biotechnol.* 36: 1211–1216.

1021

1022

1023 **Figure legends**

1024 **Figure 1. Topological analysis of FW2.2 at the plasma membrane.**

1025 **(A)** Subcellular localization of FW2.2 fused to GFP in *N. benthamiana* leaf epidermal  
1026 cells.

1027 **(B)** BiFC assays deciphering the topology of FW2.2 at the plasma membrane.  
1028 Transient expressions of FW2.2 or Lti6b fused to GFP11 and with a cytosolic GFP  
1029 (GFP1-10) or a apoplastic GFP (SP-GFP1-10) were performed in *N. benthamiana*  
1030 leaves, followed by observation using confocal microscopy Scale bar = 50  $\mu$ m.

1031 **(C)** Confocal imaging of pHGFP-PM-Apo, pHGFP-PM-Cyto and pHGFP fused to  
1032 FW2.2 at the N- and C-terminus in *N. benthamiana* leaf epidermal cells. The four  
1033 images were taken using the same confocal settings. Scale bar = 10 $\mu$ m.

1034 **(D)** 405/488 intensity ratio at plasma membrane. n>15. ANOVA followed by Tukey's  
1035 test; P < 0.05 between a and b groups.

1036

1037 **Figure 2. FW2.2 is enriched at PD.**

1038 **(A)** Confocal microscope observations of FW2.2-YFP localization in roots, pericarp  
1039 and pit field junctions in pericarp cells from 35S::FW2.2-YFP plants. Scale bar for  
1040 root and pericarp = 10  $\mu$ m. Scale bar for pit field = 5 $\mu$ m. Intensity plots delineated by  
1041 the two white arrowheads are shown for each co-localisation pattern. A.U. = Arbitrary  
1042 unit.

1043 **(B)** PD index for FW2.2 in roots and pericarp tissue of 35S::FW2.2-YFP plants  
1044 compared to WT. n>20. Statistical analysis: Student's t-test. \*\*\*\*P < 0.0001.

1045

1046 **Figure 3. The overexpression of FW2.2 enhances cell-to-cell diffusion in leaves.**

1047 **(A)** Determination of the mean mature leaf surface in WT, 35S::FW2.2 and CR-fw2.2  
1048 lines.

1049 **(B)** Determination of the cell density in leaves from WT, 35S::FW2.2 and CR-fw2.2  
1050 lines.

1051 **(C)** DANS assays using leaves from WT, 35S::FW2.2 and CR-fw2.2 lines with or  
1052 without H<sub>2</sub>O<sub>2</sub> treatment. Scale bar = 500  $\mu$ m.

1053 **(D)** Quantification of the CF signal intensity in WT, 35S::FW2.2 and CR-fw2.2 lines  
1054 with or without H<sub>2</sub>O<sub>2</sub> treatment. Statistical analysis: Kruskal–Wallis test with post hoc  
1055 Dunn multiple comparison test. \*P <0.05; \*\*\*P <0.001; \*\*\*\*P <0.0001.

1056

1057 **Figure 4. The overexpression of FW2.2 alters callose deposition in leaves.**

1058 **(A)** Immuno-labeling of callose in leaves of WT plants. Scale bar = 100  $\mu$ m.

1059 **(B)** Quantification of callose deposition in WT, 35S::FW2.2 and CR-fw2.2 lines. The  
1060 signal intensity for callose deposition is integrated to the pixel surface measured.

1061 Statistical analysis: Kruskal–Wallis test with post hoc Dunn multiple comparison test.

1062 \*\* $P$  <0.01; \*\*\* $P$  <0.001; \*\*\*\* $P$  <0.0001. n>20.

1063

1064 **Figure 5. Callose deposition is altered at 5 and 15 DPA in fruit pericarp of  
1065 35S::FW2.2 and CR-fw2.2 plants.**

1066 **(A-C)** Phenotypic analysis of fruits (at breaker stage) from 35S::FW2.2 and CR-fw2.2  
1067 plants compared to that of WT: Determination of the mean fruit weight **(A)**;  
1068 Determination of the pericarp thickness **(B)**; Determination of the number of fruit  
1069 locules **(C)**.

1070 **(D)** Immunolabeling of callose in 5 DPA (top) and 15 DPA (bottom) pericarp from WT  
1071 fruits. Scale bar = 100  $\mu$ m (top); 500  $\mu$ m (bottom).

1072 **(E-F)** Level of callose deposition in WT, 35S::FW2.2 and CR-fw2.2 lines at 5 **(E)** and  
1073 15 DPA **(F)**. The signal intensity for callose deposition is integrated to the pixel  
1074 surface measured. Statistical analysis: Kruskal–Wallis test with post hoc Dunn  
1075 multiple comparison test. \* $P$  <0.05; \*\* $P$  <0.01; \*\*\* $P$  <0.001; \*\*\*\* $P$  <0.0001. n>80.

1076 **Figure 6. FW2.2 physically interacts with several PD localized protein including  
1077 callose synthases.**

1078 **(A)** Dot plots showing enriched proteins in 35S::FW2.2-YFP IP-MS/MS experiments  
1079 in 10 DPA pericarp. Red dot indicates significantly enriched protein (based on a  
1080 Student's t-test with Benjamini-Hochberg correction  $P$  < 0.05 and an enrichment ratio  
1081 > 1.15). Blue dots indicate proteins found in the PD proteome.

1082 **(B)** Venn diagram showing the overlap between the IP-MS/MS proteome and the PD  
1083 proteome. Statistical analysis: Hypergeometric test  $P$ =0.0021.

1084 **(C)** List of plasmodesmata proteins detected in the IP-MS/ proteome.

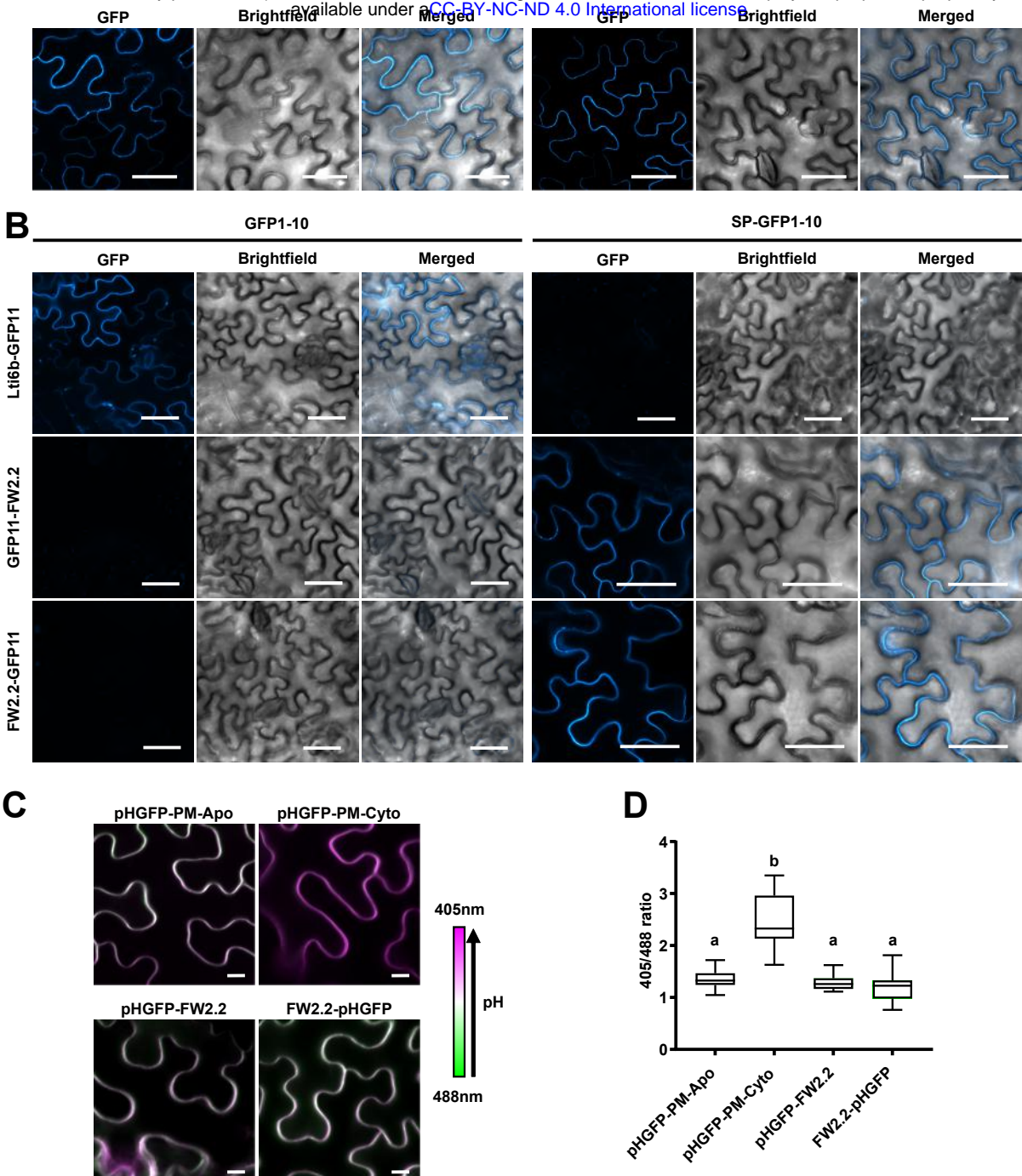
1085

1086 **Figure 7. Model illustrating the function of FW2.2 in regulating callose  
1087 synthesis at PD.**

1088 **(A)** Regulation of PD aperture by callose deposition at the neck region of PD. PD  
1089 aperture is regulated by the turn-over of callose: **(A)** a low callose deposition enables  
1090 PD opening and facilitates the traffic of signalling molecules; **(B)** callose deposition,

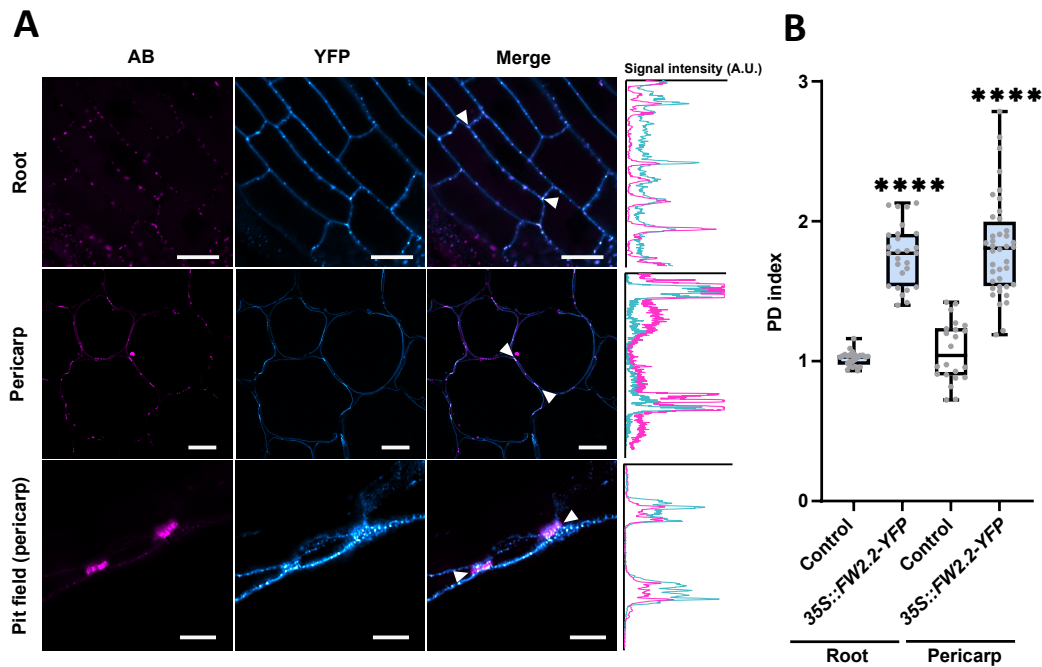
1091 enhanced by ROS ( $H_2O_2$ ) and SA, restricts the aperture of PD and the size of  
1092 signalling molecules passing through. **(C)** Molecular and cellular model for the  
1093 regulation of Callose synthase activity by FW2.2 at PD.

1094



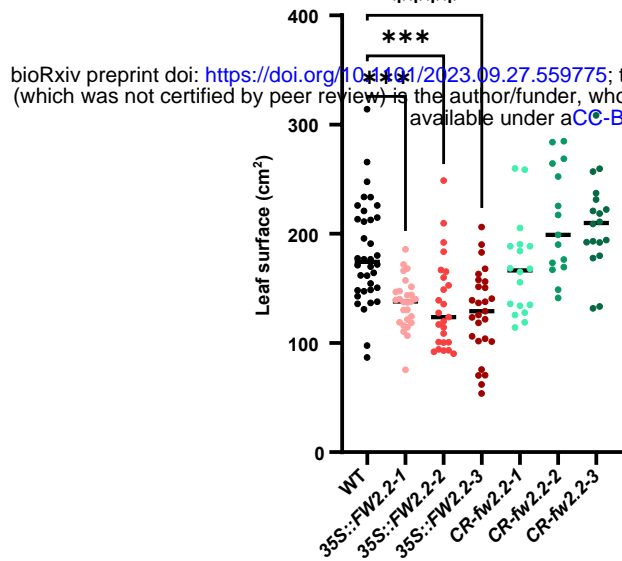
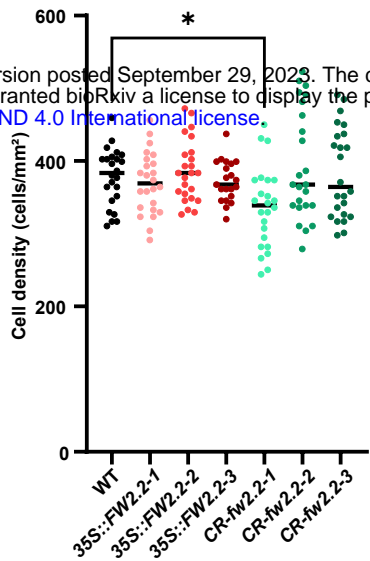
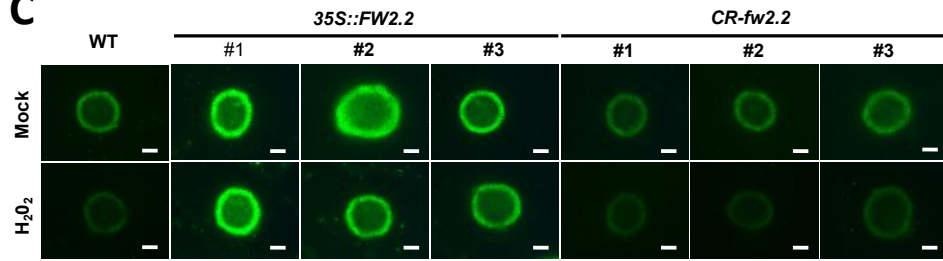
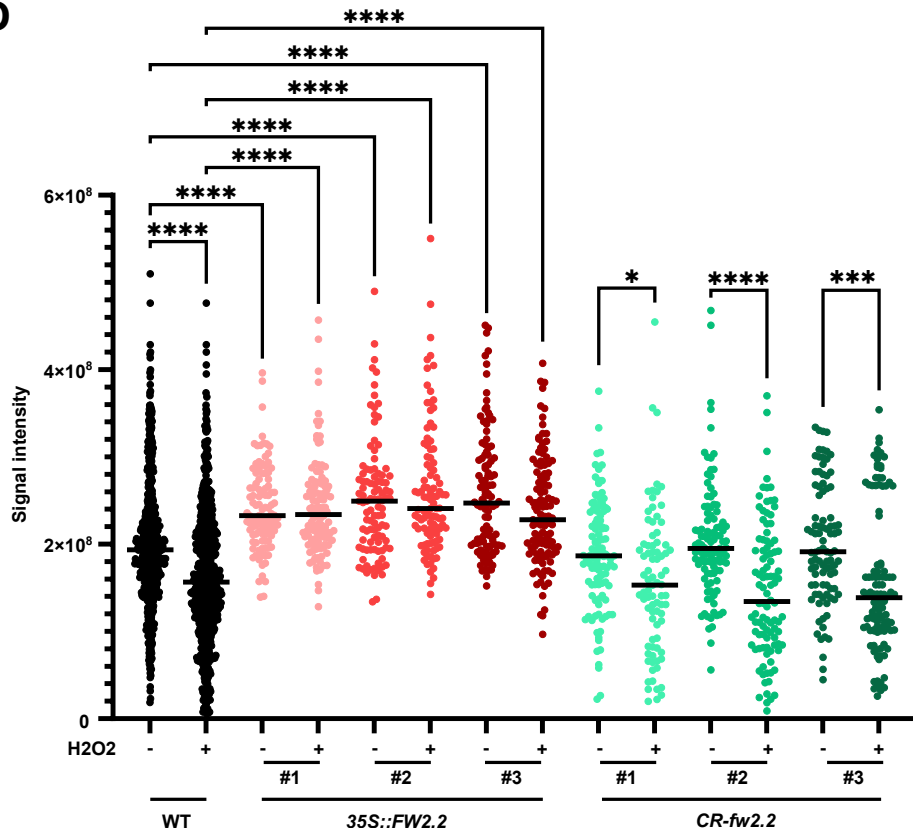
**Figure 1. Topological analysis of FW2.2 at the plasma membrane.**

**(A)** Subcellular localization of FW2.2 fused to GFP in *N. benthamiana* leaf epidermal cells. **(B)** BiFC assays deciphering the topology of FW2.2 at the plasma membrane. Transient expressions of FW2.2 or Lti6b fused to GFP11 and with a cytosolic GFP (GFP1-10) or an apoplastic GFP (SP-GFP1-10) were performed in *N. benthamiana* leaves, followed by observation using confocal microscopy. Scale bar = 50  $\mu$ m. **(C)** Confocal imaging of pHGFP-PM-Apo, pHGFP-PM-Cyto and pHGFP fused to FW2.2 at the N- and C-terminus in *N. benthamiana* leaf epidermal cells. The four images were taken using the same confocal settings. Scale bar = 10  $\mu$ m. **(D)** 405/488 intensity ratio at plasma membrane.  $n > 15$ . ANOVA followed by Tukey's test;  $P < 0.05$  between a and b groups.



**Figure 2. FW2.2 is enriched at PD.**

**(A)** Confocal microscope observations of FW2.2-YFP localization in roots, pericarp and pit field junctions in pericarp cells from *35S::FW2.2-YFP* plants. Scale bar for root and pericarp = 10  $\mu$ m. Scale bar for pit field = 5  $\mu$ m. Intensity plots delineated by the two white arrowheads are shown for each co-localisation pattern. A.U. = Arbitrary unit. **(B)** PD index for FW2.2 in roots and pericarp tissue of *35S::FW2.2-YFP* plants compared to WT. n>20. Statistical analysis: Student's t-test. \*\*\*\*P < 0.0001.

**A****B****C****D**

**Figure 3. The overexpression of FW2.2 enhances cell-to-cell diffusion in leaves.**

**(A)** Determination of the mean mature leaf surface in WT, 35S::FW2.2 and CR-fw2.2 lines. **(B)** Determination of the cell density in leaves from WT, 35S::FW2.2 and CR-fw2.2 lines. **(C)** DANS assays using leaves from WT, 35S::FW2.2 and CR-fw2.2 lines with or without H2O2 treatment. Scale bar = 500  $\mu$ m. **(D)** Quantification of the CF signal intensity in WT, 35S::FW2.2 and CR-fw2.2 lines with or without H2O2 treatment. Statistical analysis: Kruskal–Wallis test with post hoc Dunn multiple comparison test. \*P < 0.05; \*\*\*P < 0.001, \*\*\*\*P < 0.0001.

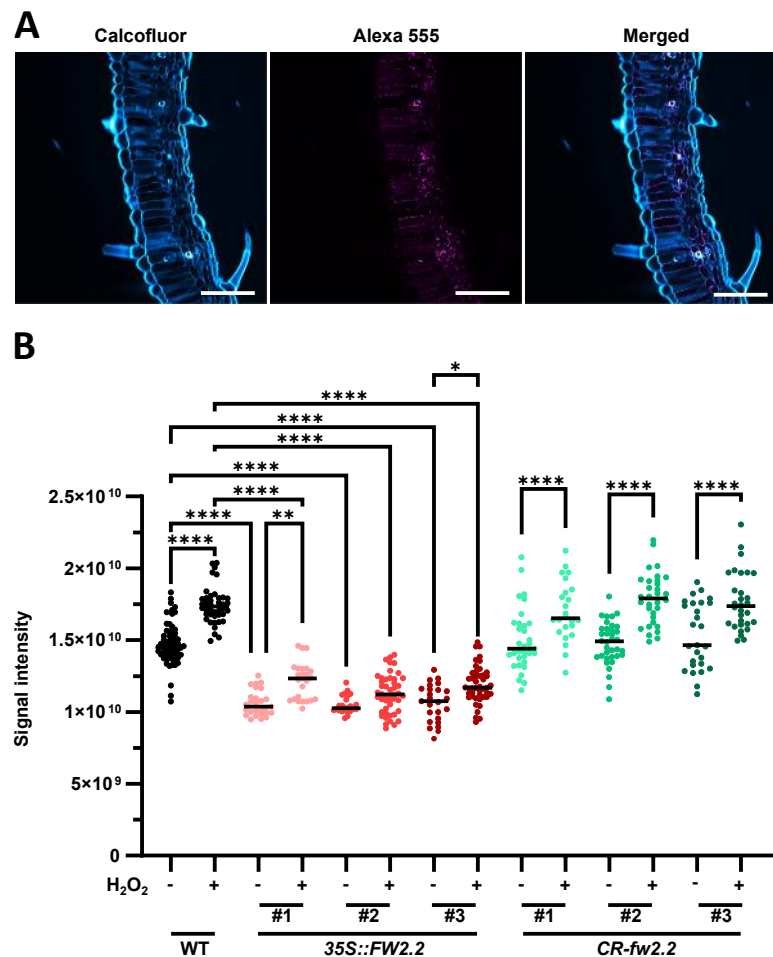


**Figure 4. The overexpression of FW2.2 alters callose deposition in leaves.**  
**(A)** Immuno-labeling of callose in leaves of WT plants. Scale bar = 100  $\mu$ m. **(B)** Quantification of callose deposition in WT, 35S::FW2.2 and CR-fw2.2 lines. The signal intensity for callose deposition is integrated to the pixel surface measured. Statistical analysis: Kruskal–Wallis test with post hoc Dunn multiple comparison test. \*\*P <0.01 , \*\*\*P <0.001, \*\*\*\*P <0.0001. n> 20.

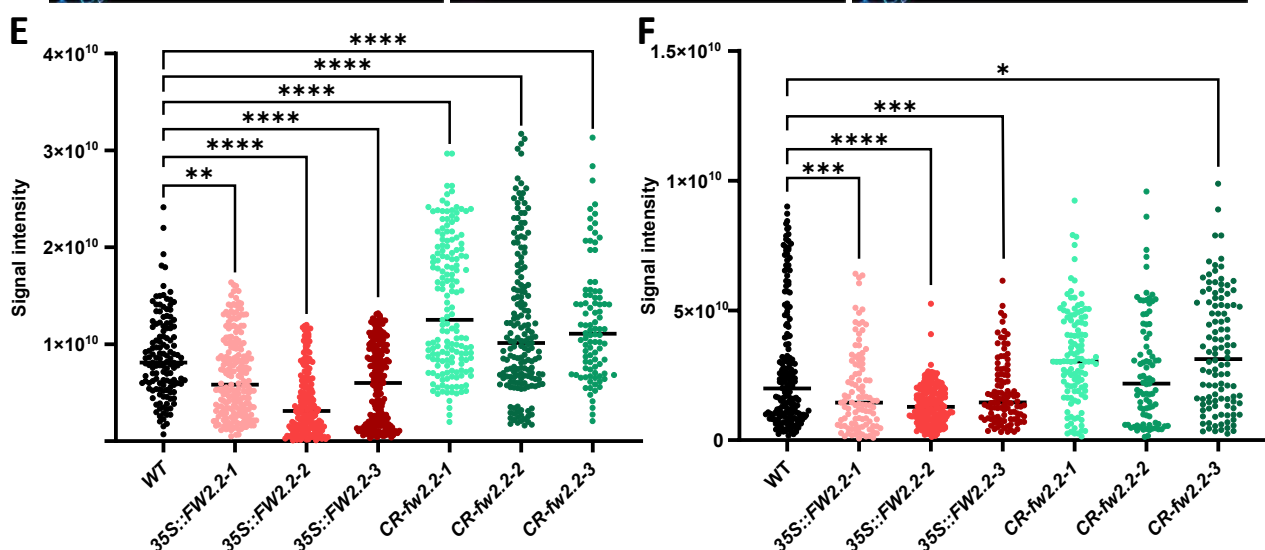
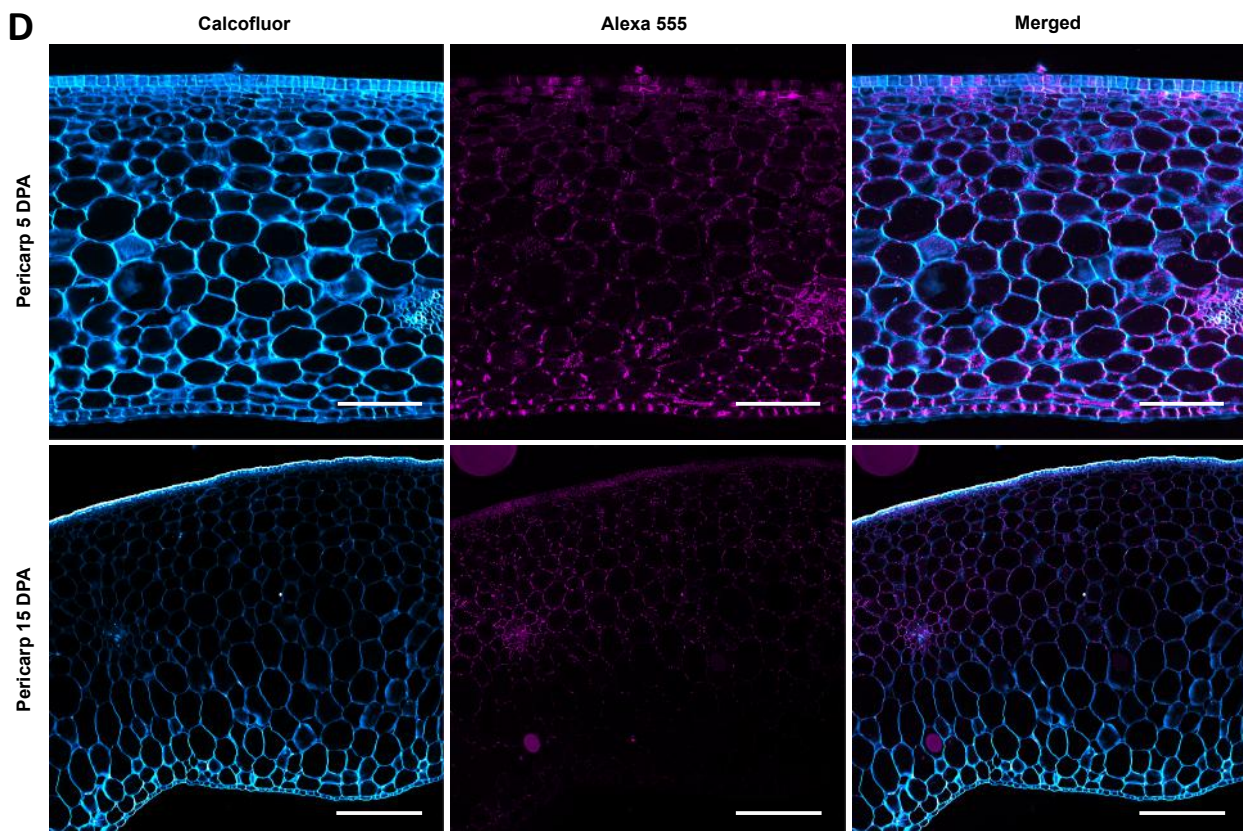
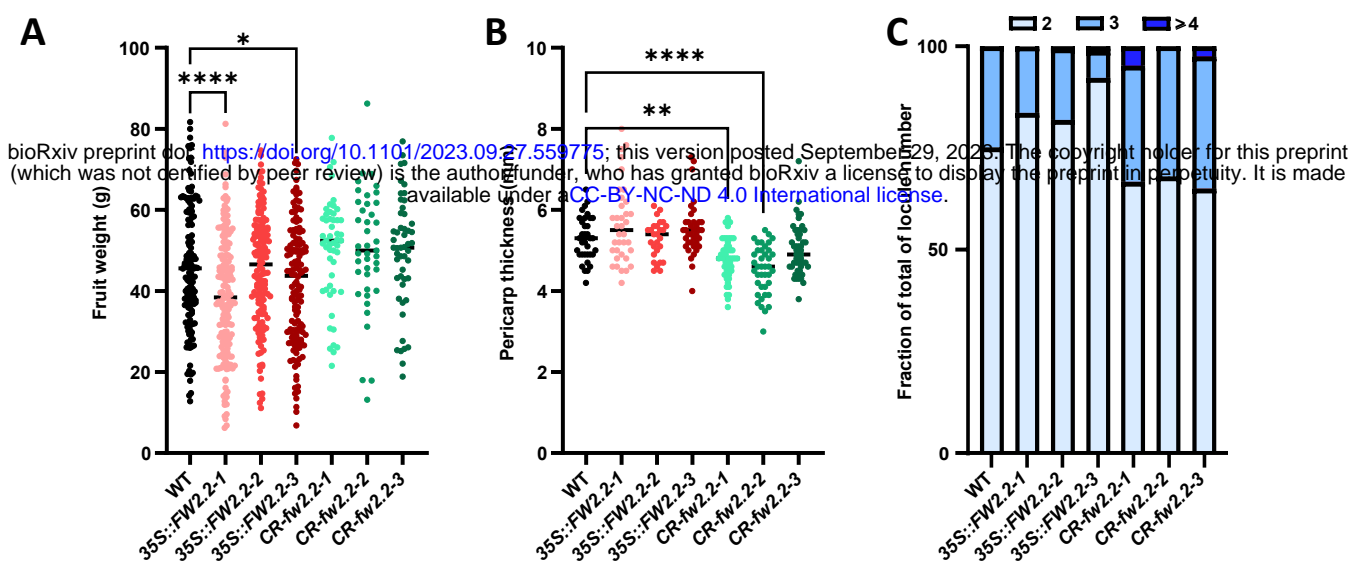


**Figure 5. Callose deposition is altered at 5 and 15 DPA in fruit pericarp of 35S::FW2.2 and CR-fw2.2 plants.**

(A-C) Phenotypic analysis of fruits (at breaker stage) from 35S::FW2.2 and CR-fw2.2 plants compared to that of WT: (A) Determination of the mean fruit weight, (B) Determination of the pericarp thickness, Determination of the number of fruit locules (C). (D) Immunolabeling of callose in 5 DPA (top) and 15 DPA (bottom) pericarp from WT fruits. Scale bar = 100  $\mu$ m (top); 500  $\mu$ m (bottom). (E-F) Level of callose deposition in WT, 35S::FW2.2 and CR-fw2.2 lines at 5 (E) and 15 DPA (F). The signal intensity for callose deposition is integrated to the pixel surface measured. Statistical analysis: Kruskal-Wallis test with post hoc Dunn multiple comparison test. \*P < 0.05; \*\*P < 0.01; \*\*\*P < 0.001, \*\*\*\*P < 0.0001. n > 80.

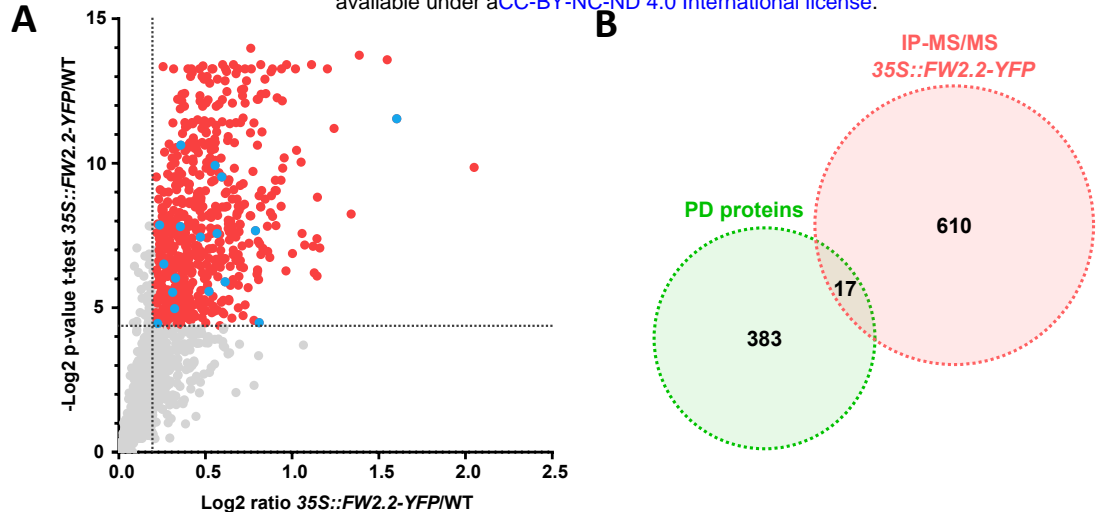
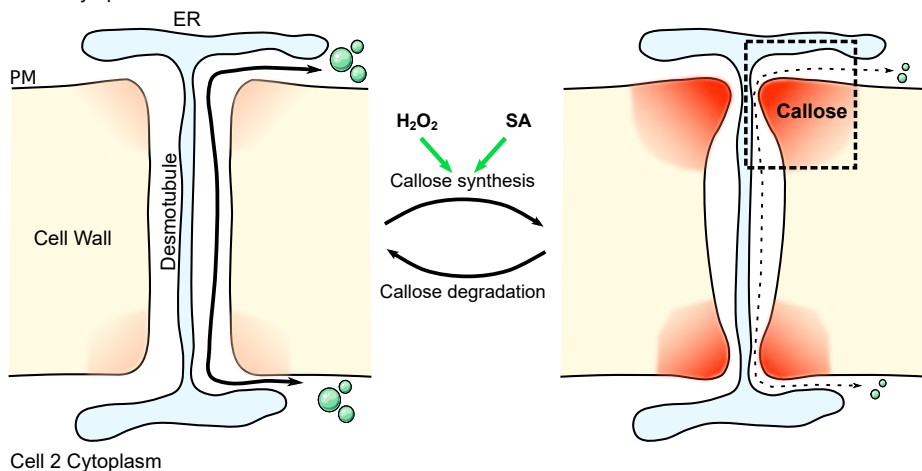


**Figure 6. FW2.2 physically interacts with several PD localized protein including callose synthases.**

**(A)** Dot plots showing enriched proteins in 35S::FW2.2-YFP IP-MS/MS experiments in 10 DPA pericarp. Red dot indicates significantly enriched protein (based on a Student's t-test with Benjamini-Hochberg correction  $P < 0.05$  and an enrichment ratio  $> 1.15$ ). Blue dots indicate proteins found in the PD proteome. **(B)** Venn diagram showing the overlap between the IP-MS/MS proteome and the PD proteome. Statistical analysis: Hypergeometric test  $P=0.0021$ . **(C)** List of plasmodesmata proteins detected in the IP-MS/MS proteome.

Cell 1 Cytoplasm

Cell 2 Cytoplasm



C

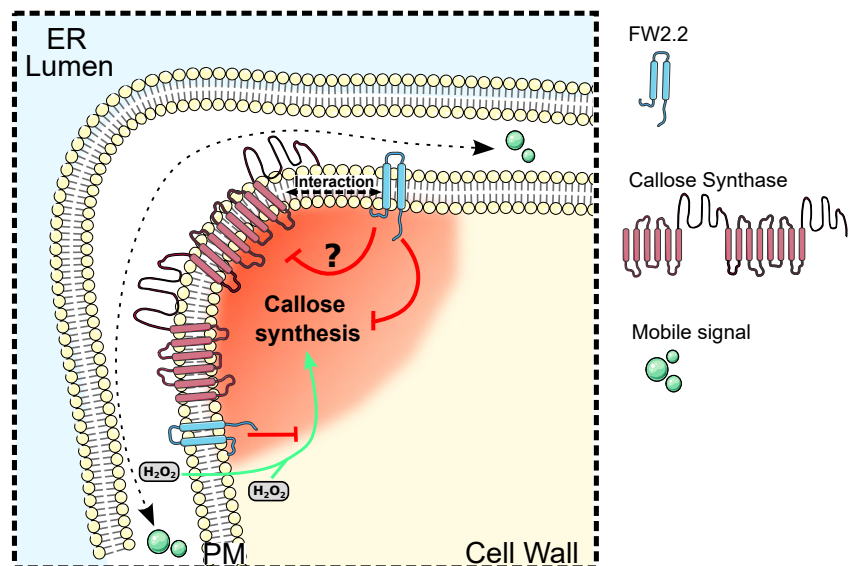


**Figure 7. Model illustrating the function of FW2.2 in regulating callose synthesis at PD.**

**(A)** Regulation of PD aperture by callose deposition at the neck region of PD. PD aperture is regulated by the turn-over of callose: (A) a low callose deposition enables PD opening and facilitates the traffic of signalling molecules; **(B)** callose deposition, enhanced by ROS ( $H_2O_2$ ) and SA, restricts the aperture of PD and the size of signalling molecules passing through. **(C)** Molecular and cellular model for the regulation of Callose synthase activity by FW2.2 at PD.

## Parsed Citations

Alpert, K. B., Grandillo, S. and Tanksley, S. D. (1995). fw2.2: a major QTL controlling fruit weight is common to both red- and green-fruited tomato species. *Theor. Appl. Genet.* 91: 994–1000.  
Google Scholar: [Author Only](#) [Title Only](#) [Author and Title](#)

Amsbury, S., Kirk, P. and Benitez-Alfonso, Y. (2018). Emerging models on the regulation of intercellular transport by plasmodesmata-associated callose. *J. Exp. Bot.* 69: 105–115.  
Google Scholar: [Author Only](#) [Title Only](#) [Author and Title](#)

Baldet, P., Hernould, M., Laporte, F., Mounet, F., Just, D., Mouras, A., Chevalier, C. and Rothan C. (2006). The expression of cell proliferation-related genes in early developing flower is affected by fruit load reduction in tomato plants. *J. Exp. Bot.* 57: 961–970  
Google Scholar: [Author Only](#) [Title Only](#) [Author and Title](#)

Beauchet, A., Gévaudant, F., Gonzalez, N. and Chevalier, C. (2021). In search of the still unknown function of FW2.2/CELL NUMBER REGULATOR, a major regulator of fruit size in tomato. *J. Exp. Bot.* 72: 5300–5311.  
Google Scholar: [Author Only](#) [Title Only](#) [Author and Title](#)

Bisbis, B., Delmas, F., Joubès, J., Sicard, A., Hernould, M., Inzé, D., Mouras, A. and Chevalier, C. (2006). Cyclin-Dependent Kinase Inhibitors are involved in endoreduplication during tomato fruit development. *J. Biol. Chem.* 281: 7374–7383.  
Google Scholar: [Author Only](#) [Title Only](#) [Author and Title](#)

Blanca, J., et al. (2015). Genomic variation in tomato, from wild ancestors to contemporary breeding accessions. *BMC Genomics* 16: 257.  
Google Scholar: [Author Only](#) [Title Only](#) [Author and Title](#)

Bollier, N. et al. (2018). At-MINI ZINC FINGER2 and SI-INHIBITOR OF MERISTEM ACTIVITY, a conserved missing link in the regulation of floral meristem termination in *Arabidopsis* and Tomato. *Plant Cell* 30: 83–100  
Google Scholar: [Author Only](#) [Title Only](#) [Author and Title](#)

Bolte, S. et al. (2004). FM-dyes as experimental probes for dissecting vesicle trafficking in living plant cells. *J. Microsc.* 214: 159–173.  
Google Scholar: [Author Only](#) [Title Only](#) [Author and Title](#)

Brandizzi F., et al. (2002). The destination for single-pass membrane proteins is influenced markedly by the length of the hydrophobic domain. *Plant Cell* 14: 1077–1092.  
Google Scholar: [Author Only](#) [Title Only](#) [Author and Title](#)

Brault, M.L. et al. (2019). Multiple C2 domains and transmembrane region proteins (MCTPs) tether membranes at plasmodesmata. *EMBO Rep.* 20: e47182.  
Google Scholar: [Author Only](#) [Title Only](#) [Author and Title](#)

Chakrabarti, M. et al. (2013). A cytochrome P450 regulates a domestication trait in cultivated tomato. *Proc. Natl. Acad. Sci. USA* 110: 17125–17130.  
Google Scholar: [Author Only](#) [Title Only](#) [Author and Title](#)

Chen, X.Y. and Kim, J.Y. (2009). Callose synthesis in higher plants. *Plant Signal. Behav.* 4: 489–492.  
Google Scholar: [Author Only](#) [Title Only](#) [Author and Title](#)

Concordet, J.-P. and Haeussler, M. (2018). CRISPOR: intuitive guide selection for CRISPR/Cas9 genome editing experiments and screens. *Nucleic Acids Res.* 46: W242–W245.  
Google Scholar: [Author Only](#) [Title Only](#) [Author and Title](#)

Cong, B., Liu, J. and Tanksley, S. D. (2002). Natural alleles at a tomato fruit size quantitative trait locus differ by heterochronic regulatory mutations. *Proc. Natl. Acad. Sci. USA* 99: 13606–13611.  
Google Scholar: [Author Only](#) [Title Only](#) [Author and Title](#)

Cong, B. and Tanksley, S. D. (2006). FW2.2 and cell cycle control in developing tomato fruit: a possible example of gene co-option in the evolution of a novel organ. *Plant Mol. Biol.* 62: 867–880.  
Google Scholar: [Author Only](#) [Title Only](#) [Author and Title](#)

Cox, J., Hein, M.Y., Luber, C.A., Paron, I., Nagaraj, N. and Mann, M. (2014). Accurate proteome-wide label-free quantification by delayed normalization and maximal peptide ratio extraction, termed MaxLFQ. *Mol Cell Proteomics* 13: 2513–2526.  
Google Scholar: [Author Only](#) [Title Only](#) [Author and Title](#)

Cui, W. and Lee, J.-Y. (2016). *Arabidopsis* callose synthases CalS1/8 regulate plasmodesmal permeability during stress. *Nat. Plants* 2: 16034.  
Google Scholar: [Author Only](#) [Title Only](#) [Author and Title](#)

Cui, W., Wang, X. and Lee, J.-Y. (2015). Drop-AND-See: A Simple, Real-Time, and Noninvasive Technique for Assaying

**Plasmodesmal Permeability.** In *Plasmodesmata: Methods and Protocols*, M. Heinlein, ed, *Methods in Molecular Biology* (Springer: New York, NY), pp. 149–156.

Google Scholar: [Author Only](#) [Title Only](#) [Author and Title](#)

**Dahan, Y., Rosenfeld, R., Zadiranov, V. and Irihimovitch, V. (2010).** A proposed conserved role for an avocado FW2.2-like gene as a negative regulator of fruit cell division. *Planta* 232: 663–676 .

Google Scholar: [Author Only](#) [Title Only](#) [Author and Title](#)

**De Franceschi, P. et al. (2013).** Cell number regulator genes in *Prunus* provide candidate genes for the control of fruit size in sweet and sour cherry. *Molecular Breeding* 32: 311–326.

Google Scholar: [Author Only](#) [Title Only](#) [Author and Title](#)

**Doganlar, S., Frary, A., Daunay, M.-C., Lester, R.N. and Tanksley, S.D. (2002).** Conservation of gene function in the Solanaceae as revealed by comparative mapping of domestication traits in Eggplant. *Genetics* 161: 1713–1726.

Google Scholar: [Author Only](#) [Title Only](#) [Author and Title](#)

**Frary, A. et al. (2000) .fw2.2 : A Quantitative Trait Locus Key to the Evolution of Tomato Fruit Size.** *Science* 289: 85–88.

Google Scholar: [Author Only](#) [Title Only](#) [Author and Title](#)

**Galaviz-Hernandez, C. et al. (2003).** Plac8 and Plac9, novel placental-enriched genes identified through microarray analysis. *Gene* 309: 81–89.

Google Scholar: [Author Only](#) [Title Only](#) [Author and Title](#)

**Gallagher, K. L., Sozzani, R. and Lee, C.-M. (2014).** Intercellular Protein Movement: Deciphering the Language of Development. *Annu. Rev. Cell Dev. Biol.* 30: 207–233.

Google Scholar: [Author Only](#) [Title Only](#) [Author and Title](#)

**Gaudioso-Pedraza, R. et al. (2018).** Callose-Regulated Symplastic Communication Coordinates Symbiotic Root Nodule Development. *Curr. Biol.* 28: 3562–3577.

Google Scholar: [Author Only](#) [Title Only](#) [Author and Title](#)

**Grandillo, S., Ku, H. M. and Tanksley, S. D. (1999).** Identifying the loci responsible for natural variation in fruit size and shape in tomato. *Theor. Appl. Genet.* 99: 978–987.

Google Scholar: [Author Only](#) [Title Only](#) [Author and Title](#)

**Grison, M. S. et al. (2019).** Plasma Membrane-Associated Receptor-like Kinases Relocalize to Plasmodesmata in Response to Osmotic Stress. *Plant Physiol.* 181: 142–160.

Google Scholar: [Author Only](#) [Title Only](#) [Author and Title](#)

**Guo, M. et al. (2010).** Cell Number Regulator1 Affects Plant and Organ Size in Maize: Implications for Crop Yield Enhancement and Heterosis. *Plant Cell* 22: 1057–1073.

Google Scholar: [Author Only](#) [Title Only](#) [Author and Title](#)

**Han, X. et al. (2014a).** Auxin-Callose-Mediated Plasmodesmal Gating Is Essential for Tropic Auxin Gradient Formation and Signaling. *Dev. Cell* 28: 132–146.

Google Scholar: [Author Only](#) [Title Only](#) [Author and Title](#)

**Han, X. et al. (2014b).** Transcription factor-mediated cell-to-cell signalling in plants. *J. Exp. Bot.* 65: 1737–1749.

Google Scholar: [Author Only](#) [Title Only](#) [Author and Title](#)

**Lemoine, F., Correia, D., Lefort, V., Doppelt-Azeroual, O., Mareuil, F., Cohen-Boulakia, S. and Gascuel, O. (2019).** NGPhylogeny.fr: new generation phylogenetic services for non-specialists. *Nucleic Acids Res.* 47: W260–W265.

Google Scholar: [Author Only](#) [Title Only](#) [Author and Title](#)

**Li, Z. and He, C. (2015).** Physalis floridana Cell Number Regulator1 encodes a cell membrane-anchored modulator of cell cycle and negatively controls fruit size. *J. Exp. Bot.* 66: 257–270.

Google Scholar: [Author Only](#) [Title Only](#) [Author and Title](#)

**Libault, M. et al. (2010).** A member of the highly conserved FWL (tomato FW2.2-like) gene family is essential for soybean nodule organogenesis: A soybean FWL essential for nodulation. *Plant J.* 62: 852–864.

Google Scholar: [Author Only](#) [Title Only](#) [Author and Title](#)

**Lippman, Z. B. and Tanksley, S.D. (2001).** Dissecting the Genetic Pathway to Extreme Fruit Size in Tomato Using a Cross Between the Small-Fruited Wild Species *Lycopersicon pimpinellifolium* and *L. esculentum* var. Giant Heirloom. *Genetics* 158: 413–422.

Google Scholar: [Author Only](#) [Title Only](#) [Author and Title](#)

**Liu, J., Cong, B. and Tanksley, S.D. (2003).** Generation and analysis of an artificial gene dosage series in tomato to study the mechanisms by which the cloned quantitative trait locus fw2.2 controls fruit size. *Plant Physiol.* 132: 292–299.

Google Scholar: [Author Only](#) [Title Only](#) [Author and Title](#)

**Marshall, O.J. (2004).** PerlPrimer: cross-platform, graphical primer design for standard, bisulphite and real-time PCR.

**Bioinformatics 20: 2471–2472.**

Google Scholar: [Author Only](#) [Title Only](#) [Author and Title](#)

**Martiniere, A. et al. (2012). Cell wall constrains lateral diffusion of plant plasma-membrane proteins. Proc. Natl. Acad. Sci. USA 109: 12805–12810.**

Google Scholar: [Author Only](#) [Title Only](#) [Author and Title](#)

**Martinière, A., Gibrat, R., Sentenac, H., Dumont, X., Gaillard, I., and Paris, N. (2018). Uncovering pH at both sides of the root plasma membrane interface using noninvasive imaging. Proc. Natl. Acad. Sci. USA 115: 6488–6493.**

Google Scholar: [Author Only](#) [Title Only](#) [Author and Title](#)

**Maule, A. J., Benitez-Alfonso, Y. and Faulkner, C. (2011). Plasmodesmata – membrane tunnels with attitude. Curr. Opin. Plant Biol. 14: 683–690.**

Google Scholar: [Author Only](#) [Title Only](#) [Author and Title](#)

**Mu, Q. et al. (2017). Fruit weight is controlled by Cell Size Regulator encoding a novel protein that is expressed in maturing tomato fruits. PLOS Genet. 13: e1006930.**

Google Scholar: [Author Only](#) [Title Only](#) [Author and Title](#)

**Nafati, M., Cheniclet, C., Hernould, M., Do, P.T., Fernie, A., Chevalier, C. and Gévaudant F. (2011). The specific overexpression of a Cyclin Dependent Kinase Inhibitor in tomato fruit mesocarp cells uncouples endoreduplication and cell growth. Plant J. 65: 543–556.**

Google Scholar: [Author Only](#) [Title Only](#) [Author and Title](#)

**Nesbitt, T.C. and Tanksley, S.D. (2001). fw2.2 Directly Affects the Size of Developing Tomato Fruit, with Secondary Effects on Fruit Number and Photosynthate Distribution. Plant Physiol. 127: 575–583.**

Google Scholar: [Author Only](#) [Title Only](#) [Author and Title](#)

**O'Lexy, R. et al. (2018). Exposure to heavy metal stress triggers changes in plasmodesmatal permeability via deposition and breakdown of callose. J. Exp. Bot. 69, 3715–3728.**

Google Scholar: [Author Only](#) [Title Only](#) [Author and Title](#)

**Park, S.J., Jiang, K., Schatz, M. C. and Lippman, Z. B. (2012). Rate of meristem maturation determines inflorescence architecture in tomato. Proc. Natl. Acad. Sci. USA 109: 639–644.**

Google Scholar: [Author Only](#) [Title Only](#) [Author and Title](#)

**Petit, J. D., Li, Z. P., Nicolas, W. J., Grison, M. S. and Bayer, E. M. (2020). Dare to change, the dynamics behind plasmodesmata-mediated cell-to-cell communication. Curr. Opin. Plant Biol. 53: 80–89.**

Google Scholar: [Author Only](#) [Title Only](#) [Author and Title](#)

**Platre, M.P., et al. (2022). The receptor kinase SRF3 coordinates iron-level and flagellin dependent defense and growth responses in plants. Nat Commun. 13: 4445.**

Google Scholar: [Author Only](#) [Title Only](#) [Author and Title](#)

**Qiao, Z. et al. (2017). The Gm FWL1 (FW2-2-like) nodulation gene encodes a plasma membrane microdomain-associated protein: A FW2-2-like protein is located in plasma membrane microdomains. Plant Cell Environ. 40: 1442–1455.**

Google Scholar: [Author Only](#) [Title Only](#) [Author and Title](#)

**Ruan, B. et al. (2020). Natural variation in the promoter of TGW2 determines grain width and weight in rice. New Phytol. 227: 629–640.**

Google Scholar: [Author Only](#) [Title Only](#) [Author and Title](#)

**Saatian, B., Kolhalmi S.E. and Cui, Y. (2023). Localization of Arabidopsis Glucan Synthase-Like 5, 8, and 12 to plasmodesmata and the GSL8-dependent role of PDLP5 in regulating plasmodesmal permeability. Plant Signaling Behav. 18: e2164670.**

Google Scholar: [Author Only](#) [Title Only](#) [Author and Title](#)

**Sicard, A., Petit, J., Mouras, A., Chevalier, C. and Hernould, M. (2008). Meristem activity during flower and ovule development in tomato is controlled by the mini zinc finger gene INHIBITOR OF MERISTEM ACTIVITY. Plant J. 55: 415–427.**

Google Scholar: [Author Only](#) [Title Only](#) [Author and Title](#)

**Song, W.-Y. et al. (2004). A Novel Family of Cys-Rich Membrane Proteins Mediates Cadmium Resistance in Arabidopsis. Plant Physiol. 135: 1027–1039.**

Google Scholar: [Author Only](#) [Title Only](#) [Author and Title](#)

**Song, W.-Y. et al. (2010). Arabidopsis PCR2 Is a Zinc Exporter Involved in Both Zinc Extrusion and Long-Distance Zinc Transport. Plant Cell 22: 2237–2252.**

Google Scholar: [Author Only](#) [Title Only](#) [Author and Title](#)

**Song L., Wang, R., Zhang, L., Wang, Y. and Yao, S. (2016). CRR1 encoding callose synthase functions in ovary expansion by affecting vascular cell patterning in rice. Plant J. 88: 620–632.**

Google Scholar: [Author Only](#) [Title Only](#) [Author and Title](#)

**Swinnen, G., et al. (2022) SIKIX8 and SIKIX9 are negative regulators of leaf and fruit growth in tomato. *Plant tPhysiol.* 188: 382-396.**

Google Scholar: [Author Only](#) [Title Only](#) [Author and Title](#)

**Tee, E. E., Johnston, M. G., Papp, D. and Faulkner, C. (2022). A PDLP-NHL3 complex integrates plasmodesmal immune signaling cascades. *Proc. Natl. Acad. Sci. USA* 120: e2216397120.**

Google Scholar: [Author Only](#) [Title Only](#) [Author and Title](#)

**Thomas, C.L., Bayer, E.M., Ritzenthaler, C., Fernandez-Calvino, L., and Maule, A.J. (2008). Specific targeting of a plasmodesmal protein affecting cell-to-cell communication. *PLoS Biol.* 6: e7.**

Google Scholar: [Author Only](#) [Title Only](#) [Author and Title](#)

**Tourdot, E., Mauxion, J.-P., Gonzalez, N. and Chevalier C. (2023). Endoreduplication in plant organogenesis: a means to boost fruit growth. *J. Exp. Bot.* erad235, <https://doi.org/10.1093/jxb/erad235>.**

Google Scholar: [Author Only](#) [Title Only](#) [Author and Title](#)

**Usak, D., Haluska, S. and Pleskot, R. (2023). Callose synthesis at the center point of plant development - An evolutionary insight. *Plant Physiol.* kiad274, <https://doi.org/10.1093/plphys/kiad274>**

Google Scholar: [Author Only](#) [Title Only](#) [Author and Title](#)

**van der Knaap, E. and Tanksley, S. D. (2003). The making of a bell pepper-shaped tomato fruit: identification of loci controlling fruit morphology in Yellow Stuffer tomato. *Theor. Appl. Genet.* 107: 139–147.**

Google Scholar: [Author Only](#) [Title Only](#) [Author and Title](#)

**Van Norman, J. M., Breakfield, N. W. and Benfey, P. N. (2011). Intercellular Communication during Plant Development. *Plant Cell* 23: 855–864.**

Google Scholar: [Author Only](#) [Title Only](#) [Author and Title](#)

**Verma, D. P. S. and Hong Z (2001). Plant callose synthase complexes. *Plant Mol. Biol.* 47: 693-701.**

Google Scholar: [Author Only](#) [Title Only](#) [Author and Title](#)

**Wang, Y., et al. (2023). Plasmodesmata mediate cell-to-cell transport of brassinosteroid hormones. *Nat. Chem. Biol.* In press.**

Google Scholar: [Author Only](#) [Title Only](#) [Author and Title](#)

**Weber, E., Gruetzner, R., Werner, S., Engler, C. and Marillonnet, S. (2011). Assembly of Designer TAL Effectors by Golden Gate Cloning. *PLoS ONE* 6: e19722.**

Google Scholar: [Author Only](#) [Title Only](#) [Author and Title](#)

**Wei, Z., Wang, J., Yang, S. and Song, Y. (2015). Identification and expression analysis of the LRR-RLK gene family in tomato (*Solanum lycopersicum*) Heinz 1706. *Genome* 58: 121–134.**

Google Scholar: [Author Only](#) [Title Only](#) [Author and Title](#)

**Weinl, C. et al. (2005). Novel Functions of Plant Cyclin-Dependent Kinase Inhibitors, ICK1/KRP1, Can Act Non-Cell-Autonomously and Inhibit Entry into Mitosis. *Plant Cell* 17: 1704–1722.**

Google Scholar: [Author Only](#) [Title Only](#) [Author and Title](#)

**Wu, J. et al. (2023). Cold stress induces malformed tomato fruits by breaking the feedback loops of stem cell regulation in floral meristem. *New Phytol.* 237: 2268–2283.**

Google Scholar: [Author Only](#) [Title Only](#) [Author and Title](#)

**Wu, S. and Gallagher, K.L. (2011). Mobile protein signals in plant development. *Curr. Opin. Plant Biol.* 14: 563–570**

Google Scholar: [Author Only](#) [Title Only](#) [Author and Title](#)

**Wu, S.-W., Kumar, R., Iswanto, A.B.B. and Kim, J.-Y. (2018). Callose balancing at plasmodesmata. *J. Exp. Bot.* 69: 5325–5339.**

Google Scholar: [Author Only](#) [Title Only](#) [Author and Title](#)

**Xie, W., Nielsen, M.E., Pedersen, C., and Thordal-Christensen, H. (2017). A Split-GFP Gateway cloning system for topology analyses of membrane proteins in plants. *PLoS ONE* 12: e0170118.**

Google Scholar: [Author Only](#) [Title Only](#) [Author and Title](#)

**Xu, J. et al. (2013). Molecular characterization and functional analysis of "fruit-weight2.2-like" gene family in rice. *Planta* 238: 643–655.**

Google Scholar: [Author Only](#) [Title Only](#) [Author and Title](#)

**Yan, D. et al. (2019). Sphingolipid biosynthesis modulates plasmodesmal ultrastructure and phloem unloading. *Nat. Plants* 5: 604–615.**

Google Scholar: [Author Only](#) [Title Only](#) [Author and Title](#)

**Zsögön, A et al. (2018). De novo domestication of wild tomato using genome editing. *Nat. Biotechnol.* 36: 1211–1216.**

Google Scholar: [Author Only](#) [Title Only](#) [Author and Title](#)

